Final Draft
of the original manuscript:

Zerbst, U.; Heinimann, M.; Dalle Donne, C.; Steglich, D.:
Fracture and damage mechanics modelling of thin-walled structures – An overview
In: Engineering Fracture Mechanics (2007) Elsevier

DOI: 10.1016/j.engfracmech.2007.10.005

FRACTURE AND DAMAGE MECHANICS MODELLING OF THIN-WALLED STRUCTURES – AN OVERVIEW

Zerbst, Uwe[a]
Heinimann, Markus[b]
Dalle Donne, Claudio[c]
Steglich, Dirk[a]

[a] GKSS Research Centre, Institute for Materials Research, Materials Mechanics, D-21502 Geesthacht, Germany

[b] Alcoa Technical Center, Product Design & Analysis, Alcoa Center, PA 15069-0001, USA

[c] EADS Deutschland GmbH, Corporate Research Centre Germany, Dept. LG-MT D-81663 Munich, Germany

1. INTRODUCTION

Thin-walled structures are important elements in many industrial areas such as aerospace, shipbuilding, bridges, industrial buildings, pipelines and others. They are frequently made of lightweight and/or high strength materials and are joined by modern welding techniques such as laser beam or friction stir welding or bonded in order to save weight. To avoid catastrophic failure, effective flaw assessment methods have to be provided which take into account characteristic features of thin-walled structures such as pronounced stable crack extension prior to fracture, the effect of stiffening elements and other items.

A number of methods have been developed for both sub-critical crack extension and final fracture of thin-walled geometries over the last decades. Some of them are already in industrial application whereas others are rather novel. But even established methods have to be re-evaluated from time to time, when new materials or design principles are introduced or when new assessment methods or advances in computer technology allow more accurate predictions.

The aim of the present paper is a brief overview of the existing methods for simulating stable crack extension and failure. Certainly it will be limited in scope and volume and not be able to fully cover the vast amount of research in fatigue and fracture of thin-walled structures over the past decades.

2. BASIC APPROACHES AND PARAMETERS

2.1 Stress Intensity Factor Concept

2.1.1 Application Range

Nowadays, the linear elastic stress intensity factor (K factor) as a parameter for describing the stress field ahead of a crack has found wide acceptance. It is applicable under small-scale yielding conditions, i.e., as long as the ligament yielding parameter L_r does not exceed a value of $L_r = 0.5$ to 0.6. The ligament yielding parameter L_r designates either the ratio of the applied

and the yield load, F and F_Y respectively, of the structure containing the crack, $L_r = F/F_Y$ or, identical to this but written in different terms, the ratio of a net section stress, σ_{ref}, and the yield strength of the material, $L_r = \sigma_{ref}/\sigma_Y$.

The yield load F_Y is the load at which the un-cracked ligament becomes plastic. It marks the change from contained to net section yielding. For non-hardening material behavior the yield load is the maximum load a cracked structure can sustain and is thus usually designated as the limit load. However, if the material work hardens the yield load does not correspond to failure, which may not occur until the plastic collapse load is reached. Whilst the determination of F_Y, or σ_{ref}, is increasingly becoming common in flaw assessment (for a more in-depth discussion see [1]) special aspects have to be taken into account for applying the concept to thin-walled structures. This will be briefly discussed in Section 3.2. If the stress intensity factor concept is applied beyond $L_r = 0.5$ to 0.6 it underestimates the crack driving force in the component, an effect which becomes dramatic for higher L_r values and which is more pronounced as the strain hardening exponent of the material gets lower, i.e. the flatter the plastic branch of the material stress-strain curve.

Whether a component fails under small-scale or contained yielding conditions depends on a number of factors such as the ductility of the material, the component dimensions, the loading case (tension or bending) and on local features such as stress concentrations or brittle zones in the material. Nowadays almost all low and medium strength structural steels used for thin wall components in shipbuilding, for bridges, pipelines etc. are rather ductile, at least for moderate loading rates. Although aluminum alloys used in aerospace are rather brittle the applicability of the stress intensity factor concept for this class of materials is limited too.

The effect of the plate thickness on the fracture resistance of an aluminium alloy 7075-T6 is illustrated in Figure 1. In this special case, for a sheet thickness smaller than ca. 3 mm, the fracture resistance in terms of K_c increases and becomes geometry dependent whereas a larger wall thickness correlates with a maximum through-thickness constraint (plane strain conditions) in conjunction with a thickness independent lower bound fracture resistance designated as K_{Ic}. Note, however, the drop in fracture resistance at very small thickness below ca. 1 mm.

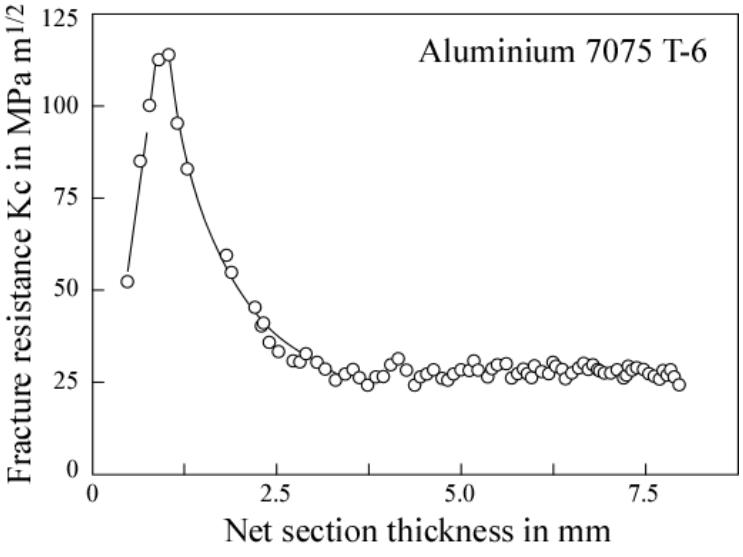

Figure 1: Variation of the fracture resistance in terms of K_c with thickness for 7075-T6 aluminium alloy (after [2]).

Several empirical equations have been introduced to correlate the geometry dependent plane stress fracture resistance, K_c, with the lower bound plane strain fracture resistance, K_{Ic}. For example, the relation

$$\frac{K_c}{K_{Ic}} = 1 + B_k \cdot \exp\left[-\left(A_k \frac{t}{t_0} \right)^2 \right] \tag{1}$$

with t being the actual plate thickness and t_0 being the plate thickness referring to ASTM E399 plane strain conditions [3]

$$t_0 = 2.5\left(K_{Ic}/\sigma_Y\right)^2 \tag{2}$$

is used in NASGRO 3.0 [4] for through crack configurations. The curve fit parameters A_k and B_k are given for a number of aerospace materials in an Appendix of the NASGRO document.

This way the geometry dependence of the material's fracture resistance is taken into account. Note, however, that there is also an effect of ligament yielding on the crack driving force in thin-walled components which frequently cannot be simply described by the stress intensity factor, at least not without a specific plasticity correction.

An extension of the application range of K is provided by the plastic zone corrected stress intensity factor K_{eff} which is obtained by replacing the real or physical crack size by a plastic-zone adjusted value a_{eff}:

$$K_{eff} = K\left(a_{eff}\right) \tag{3}$$

with the latter usually being chosen as

$$a_{eff} = a + \frac{1}{2\pi}\left(\frac{K}{\sigma_Y} \right)^2 \tag{4}$$

for plane stress conditions.

The K_{eff} concept is approximately applicable up to a ligament yielding parameter of L_r = 0.8 to 0.9. It is frequently used in conjunction with R curve analyses (see Section 2.1.3).

2.1.2 Determination of K

K factors are available as analytical solutions for many configurations, such as flat panels or cracks at holes, in handbook format or as software, or they can be obtained by finite elements or other numerical methods. Because of the requirements for sufficient stiffness, thin-walled structures are usually designed as skin-stiffener components with the stiffeners being attached by means of riveting, adhesive bonding or other joining techniques. Prominent examples are aircraft wings and fuselage structures (Figure 2).

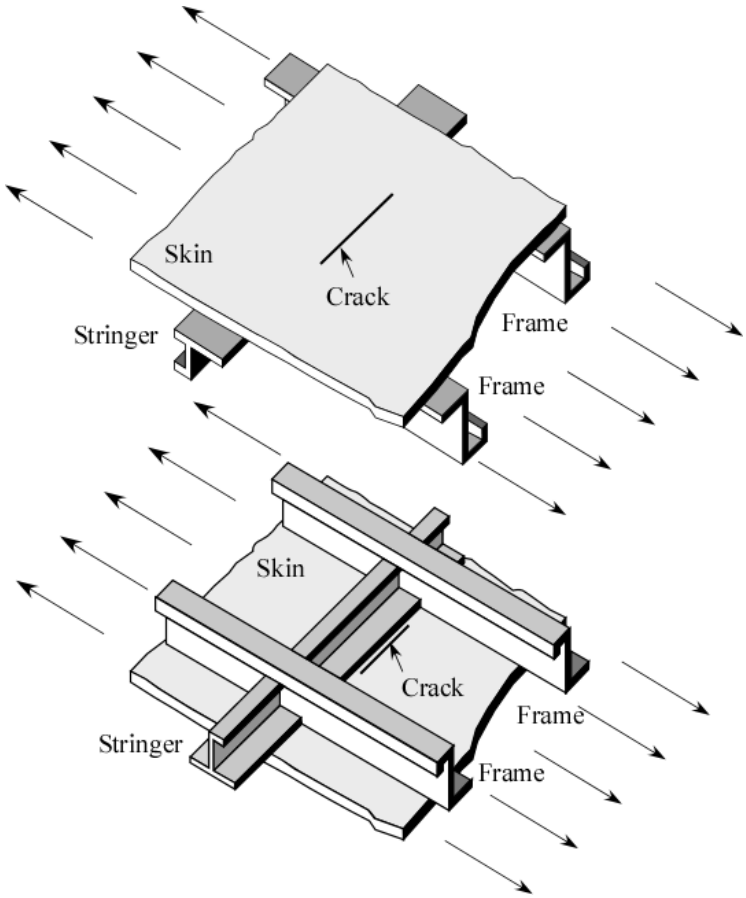

Figure 2: Typical aircraft fuselage element with a crack at the stringer.

Analytical K factor solutions for stiffened panels have already been available since the early days of fracture mechanics, for overviews see [5-7]. They are usually based on flat panel solutions extended by correction factors, ß, for the effect of the stiffeners and the bulging effect (Figure 3) due to shell curvature and, if applicable, as in the case of an aircraft fuselage, to internal pressure. An example for longitudinal cracks is the empirical curvature correction factor given below [8]:

$$\beta_{bulging} = \begin{cases} 1+\dfrac{10a}{R}\cos\left(\pi a/2L\right) & \text{crack above broken frame} \\ 1+\dfrac{10a}{R}\cdot\dfrac{1}{2}\left[1+\cos\left(2\pi a/L\right)\right] & \text{crack between intact frames} \end{cases} \quad (5)$$

with a being the half crack length, R the radius of the cylinder and L the frame spacing.

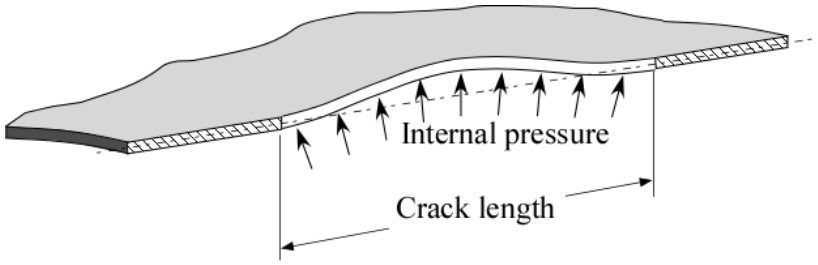

Figure 3: Bulging of the thin sheet due to shell curvature and internal pressure.

Further factors which may have to be considered are biaxial loading and details of the load transfer from the skin to the stiffener by the rivets [9-10].

Various techniques are available for deriving K by finite elements or alternative numerical techniques, such as boundary elements, from the elastic stress-strain field. They range from displacement correlation methods, to energy difference methods, to methods which correlate K to the numerically determined contour J integral. Commercial as well as in-house software codes have been developed for general and specific thin-wall applications, e.g. in the aircraft sector (see [11]). No detailed description of these methods shall be given here, for more information see [12,13].

Both the analytical and the finite element method have their specific benefits. Analytical (handbook) solutions allow an easy assessment of a varying crack size and geometrical parameters provided that these are considered adequately in the solutions. This is of benefit for structural optimization. In contrast, applying the finite element approach requires a new mesh every time the configuration is modified. The modeling effort is higher, but the finite element method allows high flexibility with respect to structural details and features such as stiffener or fastener deformation etc. which are known to be important for structural integrity, since they may affect the local constraint close to the crack tip.

2.1.3 R Curve Approach Based on K and K_{eff}

The increase in fracture resistance K_c with reduced plate thickness as shown in Figure 1 is combined with increasing crack tip plasticity and stable crack extension. Stable means that the crack is only growing when the applied load is increased and crack extension can be stopped when the load is kept constant or decreases. The specimen or component is in a stable condition. Unstable means that the crack grows without load increase. If it is not arrested after some extension it will cause the catastrophic failure of the structure. Note that stable crack extension can even occur beyond the maximum load under displacement controlled loading conditions, e.g., in a test machine. However, under stress or load controlled loading failure will always occur at maximum load. An example of stress controlled loading is internal pressure of a fuselage.

A typical feature of thin-walled geometries is the formation of shear lips and necking at the free edges of the sheet (Figure 4). Since at the center plane the constraint is higher the crack front (region 3) tends to grow there more quickly at the beginning (“tunneling effect”). The resulting crack face in region 3 is flat. Its normal coincides with the main loading direction (tensile mode) whereas, close to the free surface, shear lips form at both sides (region 4, shear mode). The shear lips show an inclination to the flat region of about 45º, but can vary due to microstructural irregularities [14]. The flat-slant transition is combined with an increase in

fracture resistance. When it, after the initial phase, reaches a steady state the crack front tends to straighten and shows what is sometimes called a “thumbnail” shape.

The fracture resistance curve (R curve) is a function of the crack tip loading in terms of K, K_{eff} or elastic-plastic parameters (see Section 2.2.2) of stable crack extension Δa (Figure 5). Krafft et al. [16] proposed to use K or K_{eff} based R curves (designated as K_R curves) instead of a geometry dependent toughness K_c or the so-called “apparent toughness” [15]. Later on it was shown for several materials that the K_R-curve for a given thickness was independent of crack size and component geometry [17].

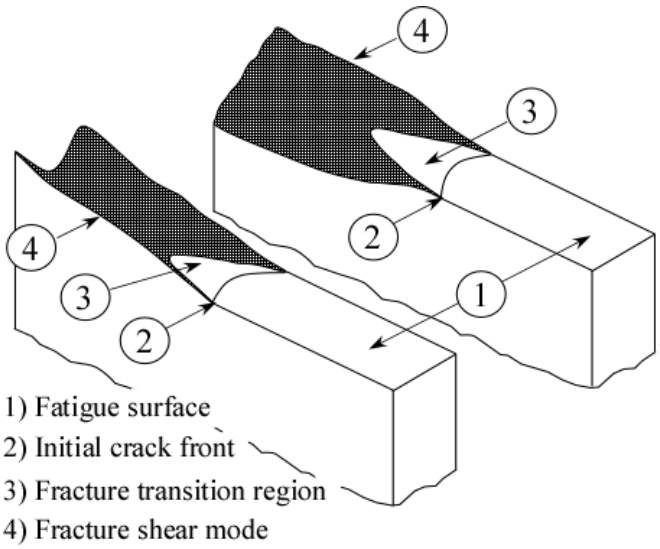

Figure 4: Crack extension with a flat-slant transition.

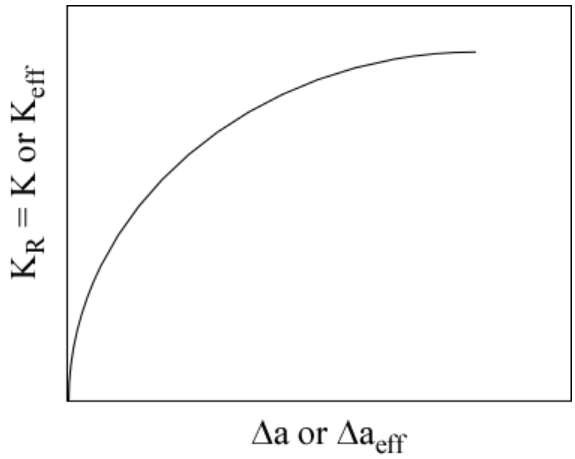

Figure 5: K_R curve (schematic).

A procedure for determining K_R curves is outlined in ASTM 561-98 [18]. Unlike other conventional test standards it does not contain minimum thickness criteria which makes it suitable for thin sheet testing. The K_R curve is determined in terms of either K_{eff} and a, or K_{eff} and a_{eff}, with a being the real (physical) and a_{eff} the plastic zone corrected crack length. The latter can be determined using Eq. (4) or, alternatively, by compliance measurements. The

shape of the K_R curve depends on the stress state at the crack tip and varies with the fracture mechanism. Whilst cleavage is combined with a flat or even falling R curve micro-ductile crack extension (microvoid coalescence) leads to a rising curve [19].

In order for the K analysis to be valid the specimen ligament ahead of the crack must be predominantly elastic. In the case of M(T) specimen configurations this is assured by the requirement that the net section stress based on the real (physical) crack size should be less than the yield strength of the material. For C(T) and C(W) specimens it is required in [18] that the remaining un-cracked ligament at the end of the test be at least equal to $(4/\pi)(K_{max}/\sigma_Y)^2$ with K_{max} designating the maximum K level in the test and σ_Y being the yield strength of the material. Following the GKSS test procedure EFAM GTP [20], and based on this the ESIS recommendation ESIS P3 [21], two criteria have to be met for a K_{eff}-R curve to be accepted:

$$F_j \leq 1.8\, B(W-a)\sigma_Y \tag{6}$$

(where F_j is either the force at termination of the test when using the multiple specimen method or the last point to be evaluated in a single specimen test) and stable crack extension Δa should not exceed the value associated with F_j for a value

$$\Delta a_{max} = 0.5(W-a_0) \tag{7}$$

(a_0 – initial crack depth) whichever is smaller.

In [22] Schwalbe et al. notice some shortcomings of the K_R curve concept. One principle drawback is that the representation of the crack by its effective size, a_{eff}, is not compatible with more recent test methods which are throughout based on the real crack size. The same is true with respect to inspecting structural components where the real crack dimensions are measured too. Furthermore, because it is based on the K_{eff} concept its range of applicability is restricted to limited ligament yielding such as outlined above. Therefore, in order to apply the method, very large specimens are required. As an example the authors in [23], investigating Al 2024-T3 Alclad sheet material, found that the panel width for obtaining valid critical K values had to be larger than 1750 mm.

What makes the method, however, even more problematic is that also the component crack driving force description in terms of K or K_{eff} is restricted to small-scale or contained ligament yielding. Increase in crack tip plasticity causes the linear elastic fracture mechanics assumptions to be non-conservative, i.e., the real crack driving force in the component is underestimated. This issue will be discussed in mode detail in Paragraph 3.2 and, dissenting to this, also in [24] in the present issue.

2.2 Elastic-Plastic Fracture Mechanics Parameters

2.2.1 General Remarks

The drawbacks of the K_r concept can be overcome by applying R curves based on elastic-plastic crack tip parameters such as the J-integral or the crack tip opening displacement (CTOD) which are not limited to small-scale yielding conditions. However, this does not necessarily mean that these parameters are suited for the application to thin-walled structures.

One severe problem is that the geometry of the thin-walled components or semi-finished products usually does not meet the thickness requirements of the common test standards such as ASTM E 1820-01 [25] or ISO 12135 [26]. These aim at plane strain conditions whereas thin-walled structures are rather subjected to plane stress conditions. Performing tests on thicker sheets and transferring the results to thin material is also not possible because the mechanical properties are altered due to the final production process, e.g., rolling.

Another problem is the pronounced stable crack extension prior to failure which usually has to be taken into account. This is particularly a problem for the J-integral which is restricted to small amounts of crack extension.

2.2.2 The Crack Tip Opening Displacement δ_5

An elastic-plastic crack tip parameter which avoids the shortcomings of the J-integral and conventional definitions of the crack tip opening displacement with respect to thin-walled geometries is the CTOD-δ_5 [27]. This parameter is uniquely defined for laboratory specimens and components by the relative displacement of two gauge points which are located 5 mm apart on a straight line going through the original crack tip (Figure 6). The parameter is determined at the plate surface(s) which might be a problem for heavy structures but not for thin sheets since plane stress conditions usually prevail across the thickness. In addition, due to the location of the gauge points, each 2.5 mm apart from the original crack tip, the δ_5 effectively averages the displacement through the wall thickness.

The δ_5 parameter has been shown to be adequate for large amounts of crack extension [27] which makes it particularly suited for thin-walled geometries. Therefore it is one of the two parameters of the ISO and ASTM draft standards for fracture mechanics testing on specimens with low constraint [22].

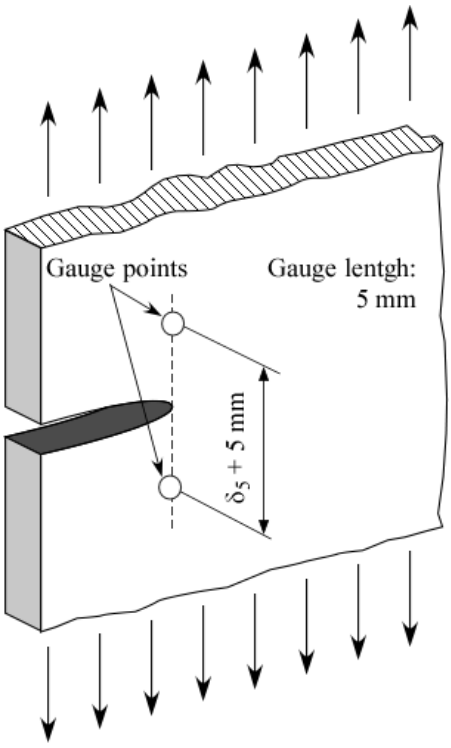

Figure 6: Definition of crack tip opening displacement δ_5.

The δ_5 gauge position does not follow the tip position of the extending crack but is stationary at the position of the original crack tip. As a consequence, it looses its meaning as a local parameter beyond a certain amount of crack growth given by

$$\Delta a_{max} = \begin{cases} 0.25\left(W - a_0\right) & \text{C(T) specimens} \\ 4 \cdot B \cdot W \cdot a_0 & \text{M(T) specimens} \end{cases} \tag{8}$$

in [20], [21] and [22].

With respect to J-integral based R curves it is well known (see [14]) that they, in principle, cannot be geometry independent. Whereas the resistance against stable crack initiation is, at least in engineering terms, broadly independent of the specimen size and type in a wide range, the slope of the R curve in any case depends on parameters such as specimen thickness, ligament slenderness and loading geometry (bending or tension) (see the overview in [28]). These dependencies are illustrated in Figure 7.

With respect to δ_5 R curves the effect of these parameters is less pronounced but, in principle, similar. Note, however, that the authors in [28], testing aluminium specimens, found upper bound R curves still dependent of thickness, B, but independent of the specimen's in plane dimensions, when the ligament width, W-a_o, was more than about 3 – 4 times the thickness. In such a case the transferability of the δ_5-R curve from specimens to large thin-walled structures is provided as long as the thicknesses of specimen and component are identical. Note, however, that this statement should not be generalized for any material. Geometry independence of the R curve has always to be checked when the method is applied to new materials. In cases where no geometry independency is found the lowest R-curve which is usually obtained by C(T) or DE(T) specimens has to be applied.

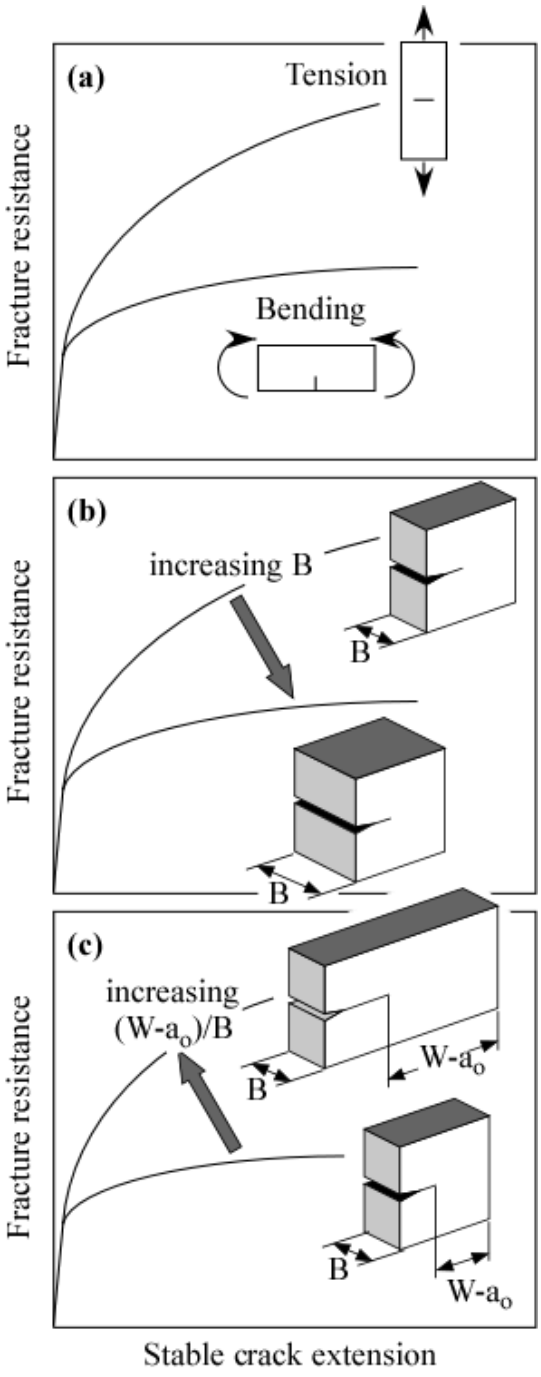

Figure 7: Factors affecting the slope of elastic-plastic R curves.

2.2.3 The Crack Tip Opening Angle ψ

The second parameter promoted by the ISO and ASTM draft standards for fracture mechanics testing on low constraint specimens [22] is the crack tip opening angle (CTOA), ψ. Anderson [29] and de Koning [30] were the first to suggest that the slope of the crack tip opening profile, the crack tip angle CTOA, could be used as a parameter characterizing stable crack extension. Later on, Demofonti and Rizzi [31] investigating ductile crack propagation in gas transmission pipelines, and Newman et al. [32], for aerospace application, found experimental evidence that the CTOA after an initial transient in the beginning of the test became almost constant for extended amounts of stable crack extension (Figure 8).

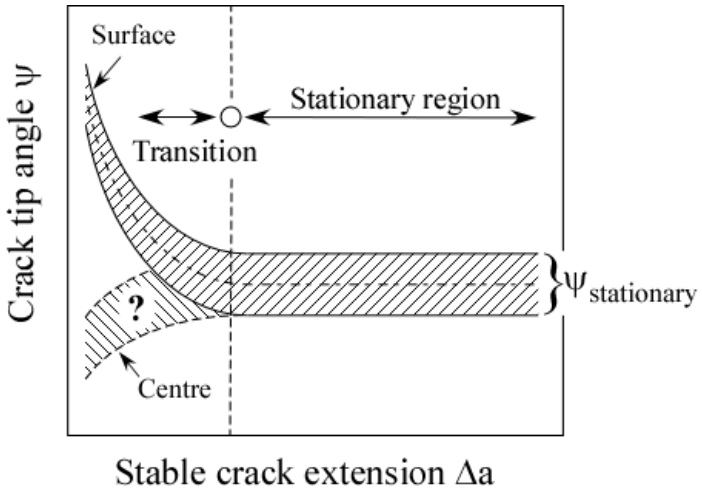

Figure 8: Development of the crack tip opening angle (CTOA) as a function of stable crack extension.

How the crack tip opening angle may be defined is illustrated in Figure 9. Generally the CTOA is the angle between the crack faces of a growing crack (Figure 9a). However, the practical realization of this straightforward definition is usually impossible because of two reasons:

(a) The definition of Figure 9a assumes straight crack faces. In reality the crack fronts are curved whereby the nature of the curvature depends on the specimen and loading type. It is, e.g., convex for M(T) and concave for bend geometries. Therefore, Kanninen et al. [33] introduced an alternative definition of the CTOA as the ratio of the crack tip opening displacement, CTOD, to a fixed distance behind the current crack tip location (Figure 9b). Sometimes the crack tip opening displacement is determined at the site of the initial crack tip (which also refers to the δ_5 definition). With increasing crack extension, i.e. increasing d in the figure this CTOA looses its meaning as local parameter and becomes different from the slope of the crack faces near the tip. In order to avoid confusion it is then designated as COA instead of CTOA. Meaningful CTOA's should be obtained for a distance d in the order of 1 mm. In any way the definition should be consistent for both experimental determination and structural assessment.

(b) A second problem is the zig-zag pattern which real crack faces show rather than the smooth shape of Figure 9b. It is, therefore, more convenient to determine CTOA's at several distinct complementary positions on the upper and lower crack surfaces, ψ_i, and to average over these values afterwards (Figure 9c). The points for determining the ψ_i values should be chosen in a range of 0.5 to 1.5 mm behind the crack tip.

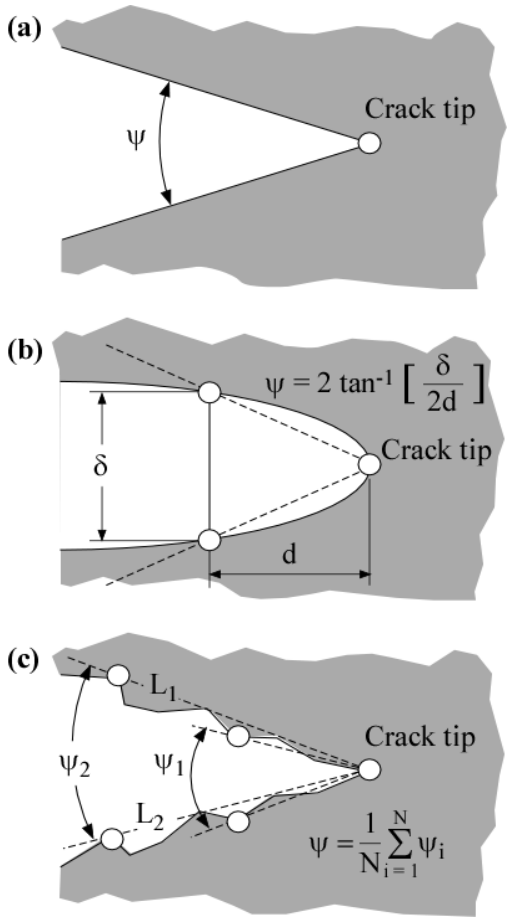

Figure 9: Definitions of the crack tip opening angle, CTOA.

The CTOA parameter has been investigated in numerous papers including a former special issue of this journal [34] and three papers of the present issue [35-37]. The following brief remarks refer mainly to these sources. Various methods are used for experimental determination of the CTOA [38]. These comprise:

(a) Optical microscopy

The crack contour close to the crack tip is investigated at the polished surface using a light microscope. A number of CTOA values is obtained at characteristic sites of the contours and averaged such as illustrated in Figure 9c. Examples are provided in [37] and [39-40]. Note, that the crack tip, due to plastic deformation of the crack faces (necking during crack extension) is frequently hard to detect. An alternative method which does not need to identify the crack tip is to connect two distinct complementary sites at each crack face by straight lines [40]. The CTOA is than the angle enclosed by the upper and lower lines, L_1 and L_2. A special case of optical measurement is the digital image correlation method [39,41-42]. In [43] the authors, following earlier attempts, use a digital camera technique for investigating relatively tough pipeline materials. In [44] moiré interferometry is used instead of light microscopy.

(b) Microtopography

By this method (see [45-46]) the fracture surfaces are topographically analyzed *post-mortem*. It is based on the assumption that the CTOA is preserved in the plastic deformations of the fracture surface. After both surfaces have been scanned they are recombined in the computer

this way reconstructing the crack contours at fracture and, based on this, the CTOA. In principle, the method allows to identify the CTOA at different thickness positions. Note that a very high accuracy in determining the topography is essential.

(c) Finite element fitting of experimental load-displacement diagrams

The experimental load displacement diagrams used are the force-Δa or the force-crack mouth opening displacement (CMOD) diagram. These diagrams are reproduced by finite element analyses using the CTOA as the controlling parameter for crack extension. When the simulated CTOA exceeds a certain value, the nodes next to the crack tip are released. The CTOA value for which the experimental maximum load is predicted is chosen as the critical CTOA, ψ_c. Note that this concept neglects the non-constant ψ during the transition phase (Figure 8). Instead, a constant value is assumed from the very beginning. Thus the finite element based ψ_c is an equivalent crack tip opening angle which should not be expected to be identical, however in the same order as the experimental stationary CTOA.

The constraint gradient in thickness direction in conjunction with the crack tunneling (Figure 4) in the early stages of crack extension and the flat-slant transition create some problems for the finite element modeling. A detailed discussion of these is provided in [38] and shall not be repeated here. Note, however, that an important conclusion of various investigations is that the analysis should not be performed for plane stress or plane strain conditions (see Figure 10) but as three dimensional analyses [47-49] or as plane stress with plane strain core analyses [11, 50]. [1)]

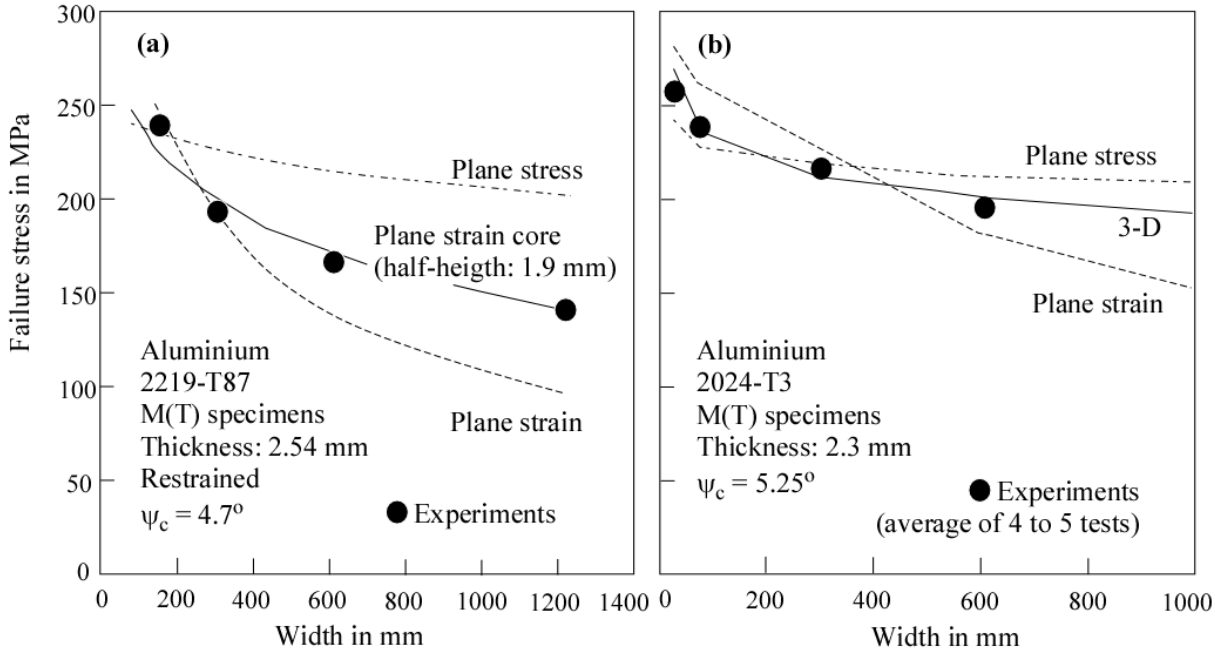

Figure 10: Experimental and predicted failure stresses of M(T) specimens as functions of specimen width. Comparison of plane stress and plane strain results with (a) plane stress + plane strain core results (after [11]) and (b) three dimensional (3-D) results (after [38]).

[1] A further indirect approach for the experimental determination of the CTOA has been developed in the context of crack arrest of pipelines made of ductile steels. The concept is based on measurements of the propagation energy [51-53].

In contrast to the finite element based ψ_c, experimental CTOA's tend to form pronounced scatter bands of up to $\pm 2^o$ or more which makes their use problematic for materials such as aluminium alloys with plateau values on the order of only 5 º to 7º. These large scatter bands cannot be reduced by more careful measurement since they are, at least partially, of physical nature: the growing crack alternately blunts and re-sharpens this way generating increases and decreases in the angle.

Like the δ_5 R curve the CTOA is dependent of the plate dimensions. This refers to both the experimental ψ values in the transition and the stationary range (see Figure 8) [54] and the ψ_c value determined by finite elements [55-56]. An example for the latter is shown in Figure 11.

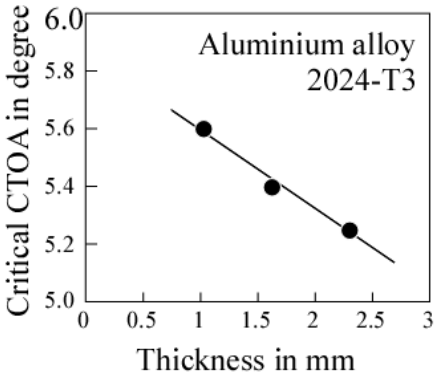

Figure 11: Influence of the specimen thickness on the critical CTOA, ψ_c (after [55]).

Studies in [56] and [57] have revealed that, for a given thickness, the CTOA was independent of specimen and loading types and specimen in-plane dimensions for cases where the crack lengths and un-cracked ligament lengths were at least four times greater than the specimen thickness. Interestingly this is the same limit value of ligament slenderness that was found for the δ_5 R-curve to be independent on the specimen's in-plane dimensions.

This raises the question whether it is possible to correlate both parameters such that δ_5 could be used to measure ψ or ψ_c in a more convenient way. Within the noticed validity limits both parameters should roughly correlate as

$$\psi = \tan^{-1}\left[\frac{d\delta_5}{d\Delta a}\right] \qquad (9)$$

which indeed was found to be the case [58] (see also Figure 12). James et al. [59-60], (see also [35]) showed that δ_5-displacement curves could be predicted by finite element analyses based on CTOA. However, due to the deviating definitions of ψ and ψ_c and due to the semi-local nature of δ_5 which combines elements of CTOA and COA the prediction of ψ from δ_5 sometimes is not accurate enough for practical application. Furthermore, Heerens et al. [37], in this issue, show that the correlation between δ_5-derived and optical CTOA is problematic for some materials since it can be significantly affected by the specimen type and material. Where discrepancies were found, these became more pronounced with increasing crack extension, i.e., in the range where the δ_5 gradually loses its meaning as a local parameter.

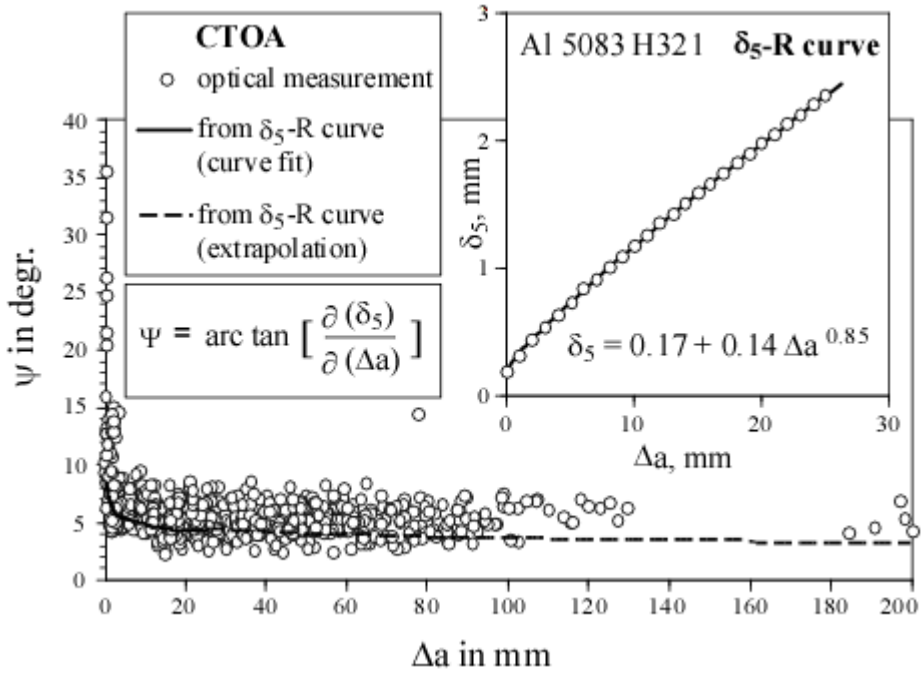

Figure 12: Comparison between optically measured and the δ_5 R-curve estimated crack tip opening angles for various specimens types and dimensions of the alloy Al 5083 H321 (after [61]).

2.3 Cohesive Zone Models

Cohesive zone models, formerly also called strip yield models, were first introduced by Dugdale [62] and Barenblatt [63]. Later Needleman was the first to use them for the analysis of crack propagation in ductile materials [64]. Recent reviews of the method are found in [65-66] and in a special issue of this journal [67]. All cohesive zone models assume a process zone ahead of the crack tip. For mode I loading the normal tensile stress T_N is correlated with a relative displacement δ_N by a specific constitutive law designated as separation law. A number of common separation laws are summarized in Figure 13. For a more comprehensive overview and the associated equations see [65] and [66]. Each separation law is characterized by its specific shape and by two limiting parameters, a maximum tensile stress T_0 and a critical displacement δ_0 after which no additional tensile stress is sustained. The area under the T-δ curves is the separation energy Γ_0. More generally the traction vector has one normal (mode I) and two tangential (modes II and III) components, each of which correspond to a separation parameter set, T_0 and δ_0. An example of a separation law used at GKSS Research Centre is given by Eq. (10) and in Figure 13f:

$$T = T_0 \begin{cases} 2\left(\frac{\delta}{\delta_1}\right) - \left(\frac{\delta}{\delta_1}\right)^3 & \delta < \delta_1 \\ 1 & \delta_1 < \delta < \delta_2 \\ 2\left(\frac{\delta-\delta_2}{\delta_0-\delta_2}\right)^3 - 3\left(\frac{\delta-\delta_2}{\delta_0-\delta_2}\right)^3 + 1 & \delta_2 < \delta < \delta_0 \end{cases} \qquad (10)$$

Setting $\delta_1 = \delta_2 = 0.33\delta_0$ Eq.(10) becomes very similar to the polynomial separation law in Figure 13 (c):

$$T = \frac{27}{4} T_0 \frac{\delta}{\delta_0}\left(1 - \frac{\delta}{\delta_0}\right)^2 . \qquad (11)$$

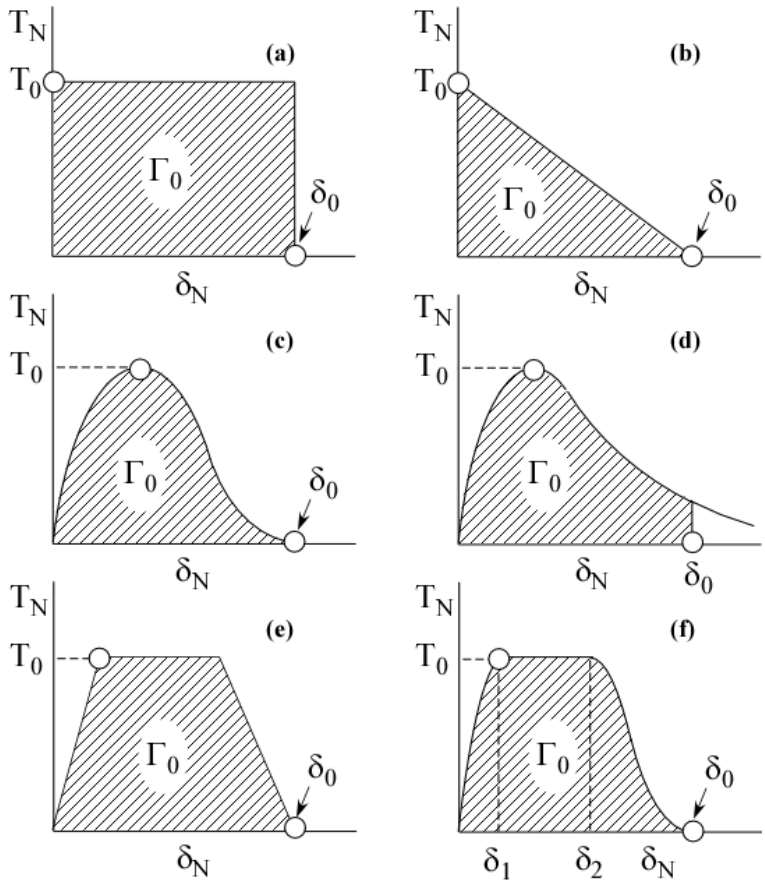

Figure 13: Cohesive zone model: Various separation laws. (a) Dugdale (1960); (b) Barenblatt (1962); Hillerborg et al. (1976) and other authors, brittle materials; (c) Needleman (1987); Tvergaard (1990); Chaboche et al. (1997), ductile materials, polynomial equation; (d) Rose et al. (1981); Needleman (1990), exponential equation; (e) Tvergaard & Hutchinson (1992); Roy et al. (2000), trapezoidal law; (f) Scheider (2000); for complete citation see [65,66].

Nowadays cohesive zone models are usually implemented as interface elements, which transfer the cohesive stress between the continuum elements. Note that the cohesive elements are two dimensional, i.e., they do not have a thickness dimension. They are introduced at the boundaries of the continuum elements. Cohesive elements are inserted either along a pre-defined crack path or along all continuum elements' boundaries within a distinct region. The latter option allows crack propagation in arbitrary directions [68,69].

The cohesive parameters T_0 and δ_0 or Γ_0 and δ_0 cannot be measured in a direct way for ductile materials but have to be identified by fitting finite element results to experimental data. These data comprise stress-strain curves of notched tensile specimens and R curves [70]. Note that

the cohesive parameters determined for different separation laws are also different, as a result they should not be regarded as model independent material parameters. They are also different for two and three-dimensional simulations (see [71] in this issue).

Cornec et al., in [70], proposed that the cohesive energy, Γ_0, as a first estimate can be taken identical to the J integral at stable crack initiation, J_i. Starting with this as a default value fine-tuning of T_0, δ_0 and Γ_0 by finite elements is usually necessary.

Although thin-walled structures generally have plane stress characteristics the application of plane shell elements in conjunction with the cohesive zone approach may not be straightforward [72]. Although its applicability has been demonstrated in some cases [77-78] care should always be exercised. Scheider et al., in [71] give an example where the modeling of a stiffened structure by shell elements would cause unrealistic results due to undue deformation of the finite elements in the stiffener region. In order to cover the effect of necking Scheider and Brocks [79] propose the use of thickness-sensitive cohesive elements for shell structures. The thickness information is taken from the adjacent shell elements and transferred to the cohesive zone elements. An illustration for the effect is provided in Figure 14.

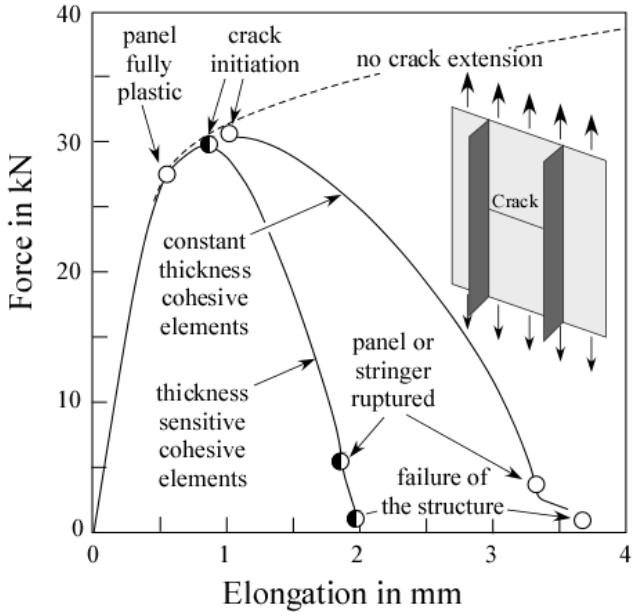

Figure 14: Load vs. elongation curves of center-cracked tensile specimens with two stiffeners obtained by constant thickness and thickness-sensitive cohesive shell elements (from [79]).

Typical 3D effects are:
- crack tunneling at the beginning of crack propagation (Figure 4) and
- necking at the panel sides during crack extension.

Three-dimensional effects were studied by various authors, on steel plates in [73] and on aluminium plates in [66,74-76]. The authors were able to simulate both the initial crack tunneling and the self-similar steady-state crack front at the later stage.

A specific question concerns the dependency of the cohesive parameters on constraint. While there seems to be only a moderate effect for high stress triaxialities this increases for low triaxialities as found in thin sheets. Siegmund and Brocks [80], using a cell model containing a void, showed that a decrease in triaxiality yields a lower cohesive strength T_0 combined

with a higher separation energy Γ_0. With respect to crack extension these two effects are expected to be contrary because of which the overall effect on the load versus stable crack extension characteristics seems to be rather moderate as it was found by a number of authors performing three-dimensional finite element analyses (e.g. [73, 75], see also [72]). Note however, that further research is necessary for a conclusive statement. In any case the fracture mechanics specimens used for parameter identification should have the same thickness as the components to be assessed.

A specific application of the cohesive element approach is its use in conjunction with R curve based models ([81]). There are cases where only relatively small specimens are available for R curve determination with the consequence that the range of valid crack extension Δa is too restricted for the application to a wide thin-walled structure. In such a case the cohesive zone model can be used for simulating R curves.

2.4 Damage Models

The problem of failure due to quasi-static loading in metals may also be approached via the methodology of constitutive equations, which include an internal variable describing the softening on a local level. The local character of the failure mechanism – deterioration of the material, which occurs prior to failure – was first accounted for by Kachanov [82] by introducing an internal scalar field variable. Later, "local approaches" and "micromechanical modeling" of damage and fracture [83-85] have found increasing interest and application. Generally, the “local approach” is based on finite element simulations of stress and strain fields. So-called locally coupled models [84] are based on a rather simple elastic–plastic calculation with post-processing and can be used to predict crack initiation. Fully coupled models account for the softening effect induced by cavity growth (in the case of ductile fracture), micro cracking or decohesion between aggregates. These models use internal variables (scalars, vectors or tensors) to quantify the amount of damage at a material point. An evolution equation for the damage variable has to be formulated and a correlation between damage variable and stresses and strains has to be established. This can be done via a purely phenomenological procedure by postulating thermodynamic potentials [86, 87] or via a homogenization method [88-90], which may account for the micromechanical mechanisms of damage [91, 92]. In the first case the damage variable is solely used to describe the influence of deterioration on the stresses and a physical interpretation of the variable can only be given as a vague approximation. In the second case a representative volume element (RVE) has to be defined and constitutive relations have to be derived on a "meso-scale" by a homogenization method. In this class of models, probably the most famous is the one from Gurson, Tvergaard and Needleman, the so-called GTN model [93]. It can be seen as an extension of the von Mises yield criterion by an additional variable, f^*, damage, which is combined with the stress triaxiality as

$$\Phi = \frac{\sigma_{eq}^{\,2}}{R^2(\bar{\varepsilon})} + 2q_1 f^* \cosh\left[\frac{q_2}{2}\frac{\sigma_{kk}}{R(\bar{\varepsilon})}\right] - 1 - q_3 f^{*2} = 0 \qquad (12)$$

in the second term, giving the yield condition for a porous metal.

The approach of continuum damage mechanics may be seen as a way to overcome the numerous problems of size and geometry dependence of the fracture parameters used in conventional fracture mechanics. In fact, numerous successful applications of damage models of the “porous metal plasticity” family exist via the implementation in the framework of finite elements [94-97]. The models were used for the assessment of thick-walled geometries, where a high constraint causes a high triaxiality and thus void growth has a significant effect on the

stress carrying capacity of a material point. In the context of sheet metal and thin-walled structures, however, the applications are scarce. This may be due to the fact that the triaxiality is limited by the value of 0.66 for plane stress states and thus damage evolution is deferred compared to thick-walled components [98]. Hence, the complex conditions ahead of an extending crack have to be modeled using a 3D-discretisation of the process zone [99], which limits the general advantage of using one material model for the description of the mechanical behavior of a single material. The partitioning into a 3D-process zone and shell-like structural part obeying plane stress conditions is a common technique, which is adopted using CTOA concept, cohesive elements as well as the X-FEM or G-FEM (see Wyart et al. [100] in this Special Issue).

Provided that the failure mechanisms do not change for a given material and prescribed conditions, models accounting for both void nucleation and growth allow describing size and geometry effects [19, 101] which are often encountered when trying to transfer parameters from laboratory specimens to structures [102].

Another interesting feature is the capability of describing the fracture mode: flat or slanted. It was shown in [103] that the transition from flat to a slanted fracture can be modeled using the Rousselier model, but in this particular case the global behavior of the test specimen in terms of load-displacement and crack growth rate was not met. The flat to slant crack path change is the subject of ongoing research. Currently, focus is put on the prediction of the macroscopic behavior [104], even if the fracture surface remains flat in the simulations.

3. APPLICATION TO RESIDUAL STRENGTH SIMULATION

3.1 Residual Strength

The term “residual strength”, as frequently used in aerospace applications, designates the load carrying capacity of a cracked structure as a function of the material toughness, the crack size and geometry and the structural configuration [105]. The principle is illustrated in Figure 15. For linear elastic conditions the crack driving force in the component is provided in terms of the K factor and the residual strength is simply determined by equation 13,

$$\sigma = K \big/ \sqrt{\pi a}\, Y \tag{13}$$

Where a is the crack length and Y the geometry function of the component. For elastic-plastic conditions the relation between crack driving force and residual strength becomes more complicated.

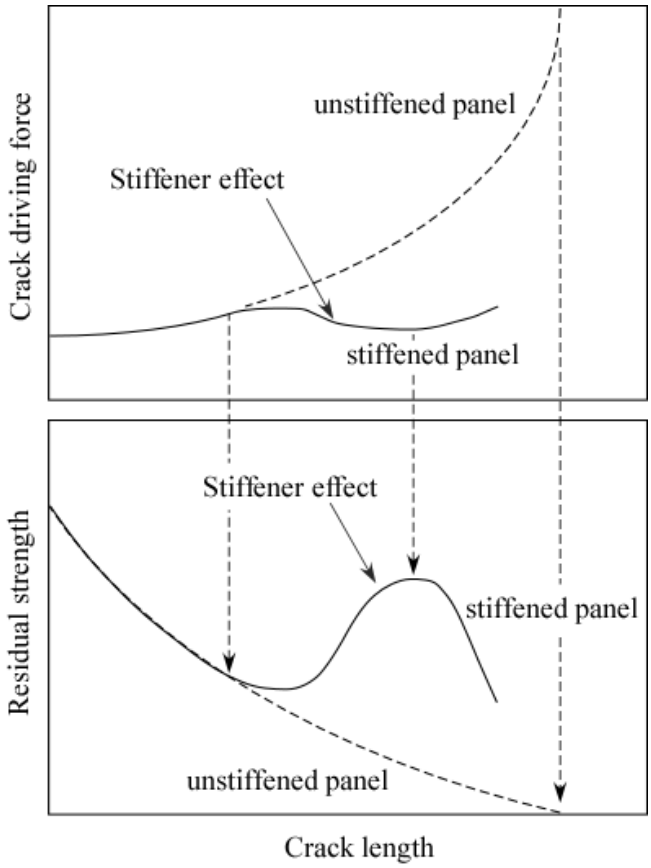

Figure: 15: Basic principle of a residual strength diagram.

When the crack, during its extension, passes a stiffener area the crack driving force is decreased compared to the un-stiffened case (load shielding effect) and the residual strength increases. An example of a more complex residual strength diagram of a built-up structure is provided in Figure 16 [5] where two limit curves, one for the skin and the other for the stiffener, are shown along with their interaction. Failure occurs when either the skin or the stiffener fails. Note that an exact residual strength (and the same is true with respect to an exact crack driving force) requires sophisticated analyses, e.g., taking into account the load transfer characteristics of the joint, e.g., rivet or bond. The effect of the number of fasteners taken into account in an analysis is illustrated in Figure 17 as an example.

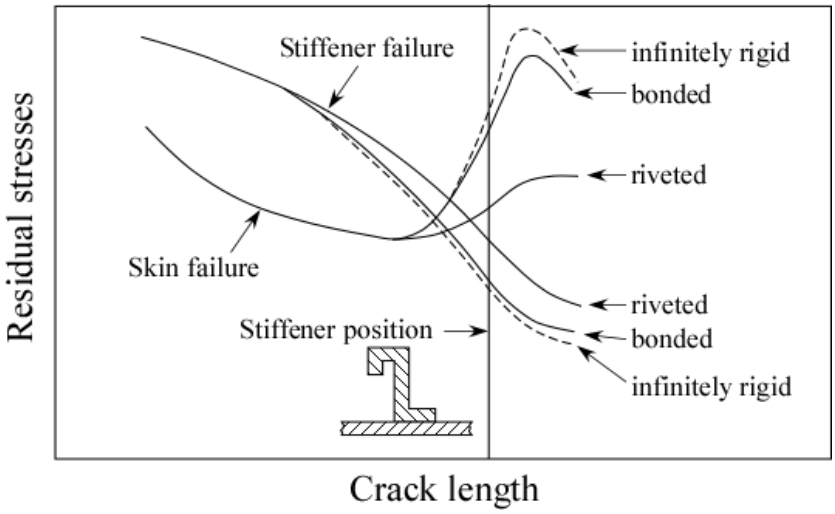

Figure 16: Residual strength diagram of a built-up structure (after [5]) comparing riveted and bonded realizations.

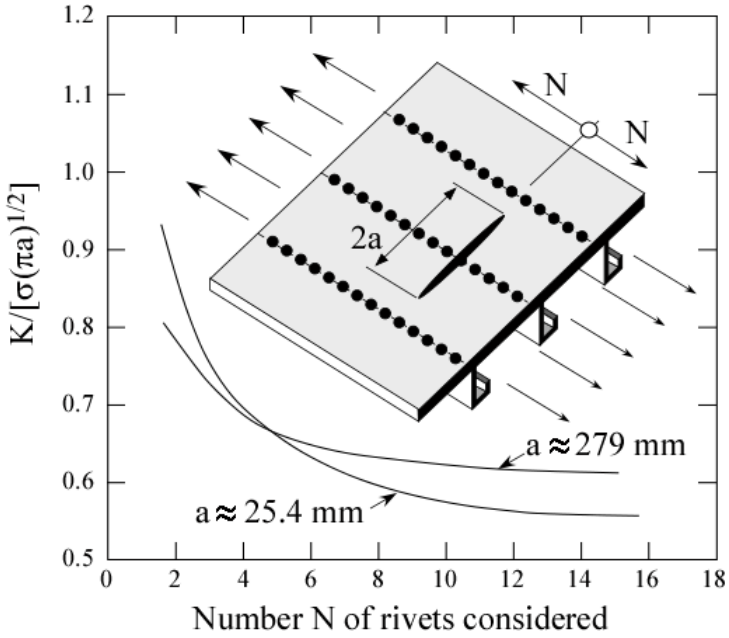

Figure 17: Effect of the number of fasteners included in stress intensity factor analysis (after [5]).

3.2 Application of the R curve Approaches to Panels and Stiffened Shell Structures

The application of the R curve approach to structural assessment is illustrated in Figure 18. The crack driving force versus crack depth functions (in terms of K, K_{eff} or δ_5) are plotted for different constant applied loads (in the figure: loads 1, 2 and 3) together with the R curve of the material. The load whose crack driving force curve is tangent to the R curve is the instability load of the structure under stress controlled loading. Note that the crack driving force at instability is always geometry dependent, i.e. it is a material and component specific parameter and does not refer to the fracture resistance at the maximum load in a test specimen. Diagrams like that of Figure 18 can be used for assessing the effects of various

parameters on the instability load such as demonstrated in Figure 19 for an improved R curve behavior (Figure 19a) and for a smaller original crack depth in the component (Figure 19b). The latter could be the benefit of an improved non-destructive inspection strategy. In addition to the critical load, the crack size at instability and the corresponding stable crack extension can be determined by this type of diagram.

An alternative R curve approach is illustrated in Figure 20.

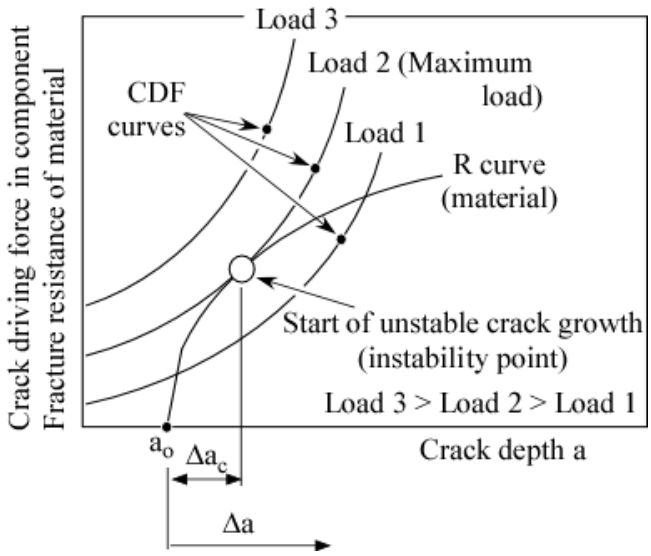

Figure 18: R curve analysis for determining the instability load of a structure (schematic).

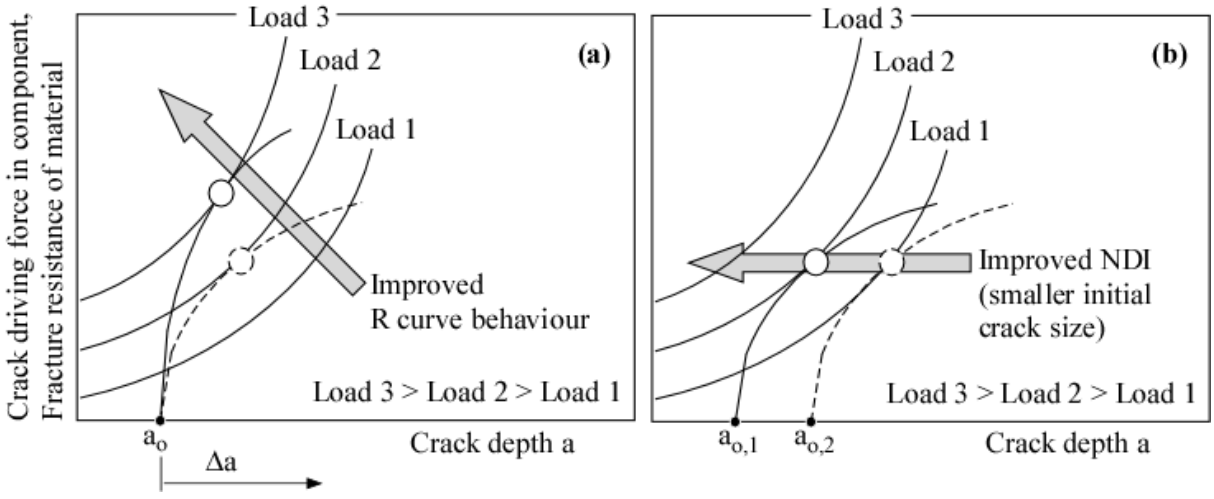

Figure 19: The effect of various parameters on the instability load of the component, (a) Fracture resistance of the material (steepness of the R curve); (b) Original crack depth a_0 in the component.

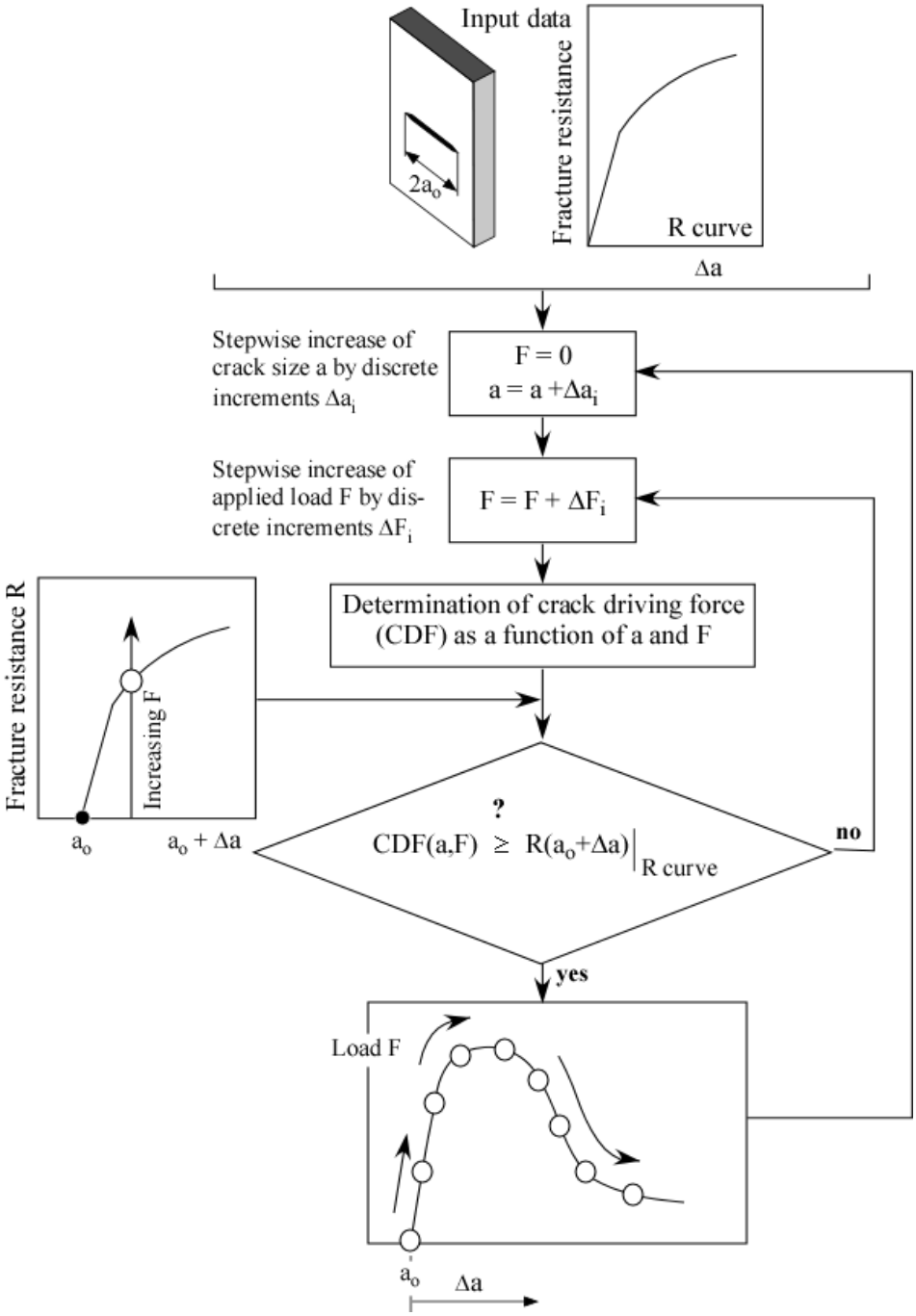

Figure 20: Flow chart for determining the applied load versus stable crack extension characteristics (after [61]).

In Paragraph 2.1.3 it was mentioned that a serious problem of the K_R curve approach even on the basis of K_{eff} is its restriction to limited crack tip plasticity with the application range is limited by ligament yielding smaller than L_r = 0.8 to 0.9, see also the discussion of Ehrström in this issue [24]. Unfortunately neither the information on this limit nor its identification in real structures are implicit parts of the existing methodology. This does not mean that the common K_R curve method is not a useful tool for residual strength determination of thin-walled structures. It means, however, that its applicability for a specific material and/or component has to be proven prior to industrial application. An example of such an experimental verification is provided in [106].

An alternative option is to replace the K_R approach by more up-to-date methods such as R6 [107], BS 7910 [108] or SINTAP/FITNET [1] (for a detailed description see [1]) which are not limited to small scale yielding but applicable up to plastic collapse. Particularly the SINTAP/FITNET method contains a special thin-wall option which shall be briefly explained in the following paragraphs.

The SINTAP/FITNET thin wall module can be applied in conjunction with an R curve approach based on the δ_5 specification of the CTOD such as described in Paragraph 2.2.2. The δ_5 R-curve has to be obtained on specimens of component thickness with crack lengths, a, and initial un-cracked ligament lengths, W-a, being equal or greater than four times the thickness.

Within the SINTAP/FITNET approach crack driving force functions are given by

$$\delta_5 = \delta_e \cdot \left[f\left(L_r\right) \right]^{-2} \tag{14}$$

with

$$\delta_e = K^2 / \left(E' \cdot \sigma_Y \right). \tag{15}$$

Note that the term $f(L_r)$ can be interpreted as a "ligament yielding correction" for K. Depending on the quality and completeness of the input information various analysis levels with different $f(L_r)$ solutions are available. Here, only the standard option $f(L_r)$ for materials without a yield plateau shall be presented. For the other options the reader is referred to [1]. The function is given by:

$$f\left(L_r\right) = \begin{cases} \left[1 + 0.5 \cdot L_r^2 \right]^{-1/2} \cdot \left[0.3 + 0.7 \cdot \exp\left(-\mu \cdot L_r^6 \right) \right] & \text{for } 0 \le L_r \le 1 \\ f\left(L_r = 1\right) \cdot L_r^{(N-1)/2N} & \text{for } 1 < L_r \le L_r^{max} \\ 0 & \text{for } L_r > L_r^{max} \end{cases} \tag{16}$$

with

$$\mu = \min \begin{cases} 0.001 \left(E / R_{p0.2} \right) \\ 0.6 \end{cases}, \tag{17}$$

and $L_r = F/F_Y$ or σ_{ref}/σ_Y (as already mentioned in Paragraph 2.1.1) being given in compendia (e.g. [107-109]) for standard geometries. N designates the strain hardening coefficient and L_r^{max} the plastic collapse limit.

In Figure 21 a comparison is provided between the crack driving force in terms of K, K_{eff} and K_p according to SINTAP/FITNET for an M(T) specimen of an aluminium alloy. The index "p" stands for "plasticity corrected". Note that K_p is not SINTAP/FITNET nomenclature. The parameter $K_p = 1/f(L_r)$ is used instead of δ_5 but compatible with Eq. (14). It can be seen that the more realistic crack driving force K_p is underestimated by K_{eff} and even more by K. Note that the difference becomes larger with increasing L_r and particularly above $L_r = 1$.

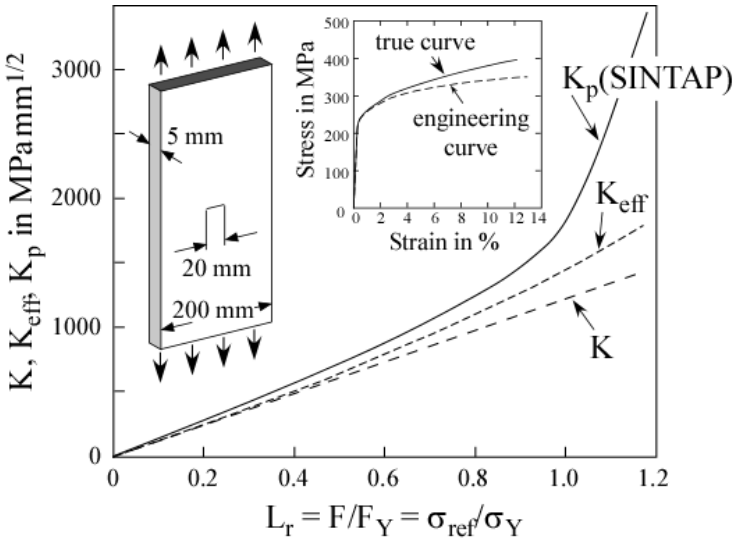

Figure 21: Comparison of the crack driving force in terms of K, K_{eff} and K_p (the latter being determined by SINTAP/FITNET, Option 3) as a function of ligament yielding L_r.

Since thin sheets are usually manufactured by rolling, they tend to be anisotropic with respect to their tensile properties. Two examples of aluminium alloys are provided in Figure 22. Anisotropy has to be taken into account by all concepts introduced in Paragraph 2 except those based on linear elastic K factor solutions without plastic zone correction. The SINTAP/FITNET thin wall option recommends the use of the lowest stress-strain curve for determining the crack driving force.

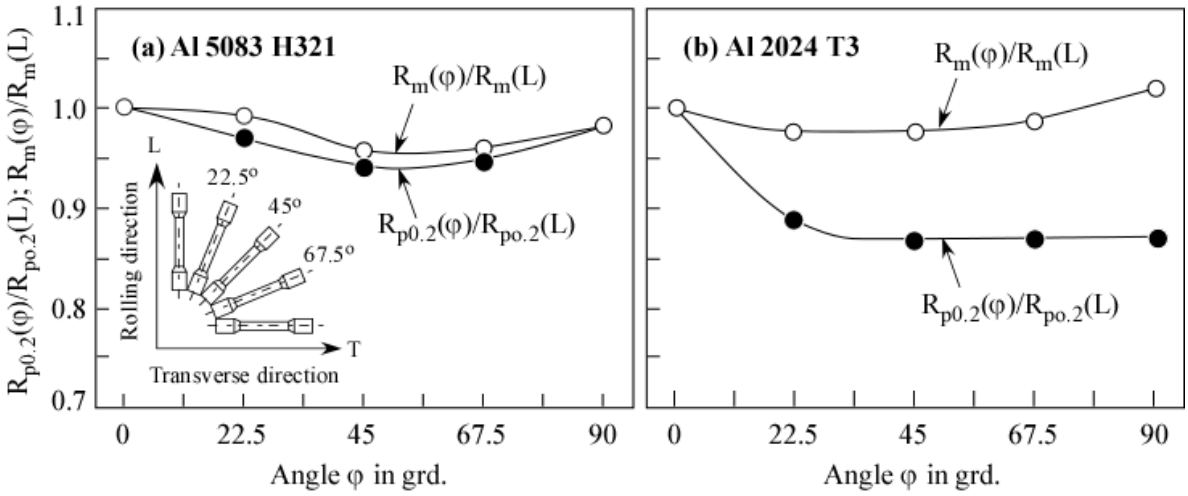

Figure 22: Tensile properties as a function of specimen orientation for two aluminium alloys (after [110]).

In order to avoid extrapolation of the δ_5-Δa curve beyond its validity limits the stable crack extension Δa at the maximum load in the component should not exceed the Δa range which is covered by the experimental R-curve. Examples of SINTAP/FITNET predictions of maximum loads in thin-walled panels under biaxial tension loading are shown in Figure 23. For more detailed information see [110]. Note that the SINTAP/FITNET approach also

provides guidance to account for welding residual stresses and strength mismatch (see Paragraph 3.4.4).

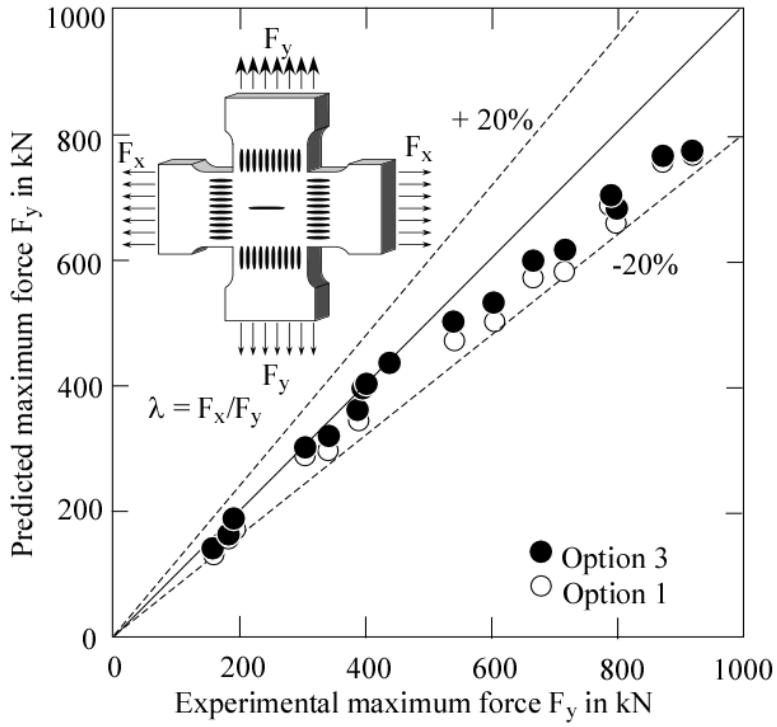

Figure 23: SINTAP/FITNET thin wall option: Predicted and experimentally determined failure loads of biaxially tension loaded plates (after [110]). The data set includes different materials and biaxiality ratios $\lambda = F_x/F_y$ of –0.5, 0, +0.5 and +1.

Panels without stiffeners are the simplest thin-walled components and K factor as well as yield load solutions are available in handbook format. However, real thin-walled geometries are frequently not flat panels but stiffened structures and often curved shells for which no analytical yield load or L_r solutions and sometimes even no analytical K factor solutions are available. In such cases the input parameters can be determined by finite elements or alternative methods and can then be used within the frame of the K_R curve or, better the SINTAP/FITNET concept. A simple example for such a hybrid approach is illustrated in Figure 24 [111]. In a first step K factor and yield load (F_Y) solutions have been determined for various crack lengths by finite elements. These solutions were then used to predict load versus crack size curves following the method of Figure 20. By repeating this exercise for different initial crack lengths the authors obtained the shown residual strength diagram. As expected, the residual strength decreases with increasing crack length and reaches a minimum at some distance from the stiffener. For larger crack lengths it increases again as a consequence of the load shielding effect of the stiffener.

A specific problem with respect to thin-walled structures is the definition of an appropriate yield load F_Y or the assocuated L_r parameter. The common large in-plane dimensions of thin sheets require the use of what is called a “local” yield load. In contrast to the “global” yield load this term refers to the yielding of a local ligament area which is hard to define. In [111] the authors obtained the yield load as the load referring to a δ_5/δ_e ratio of 2.12 in accordance with a value $L_r = 1$ in Eq. (14). Both δ_5 and δ_e have been determined by finite elements. Note,

however, that further investigations are needed in order to substantiate and validate this kind of hybrid approach.

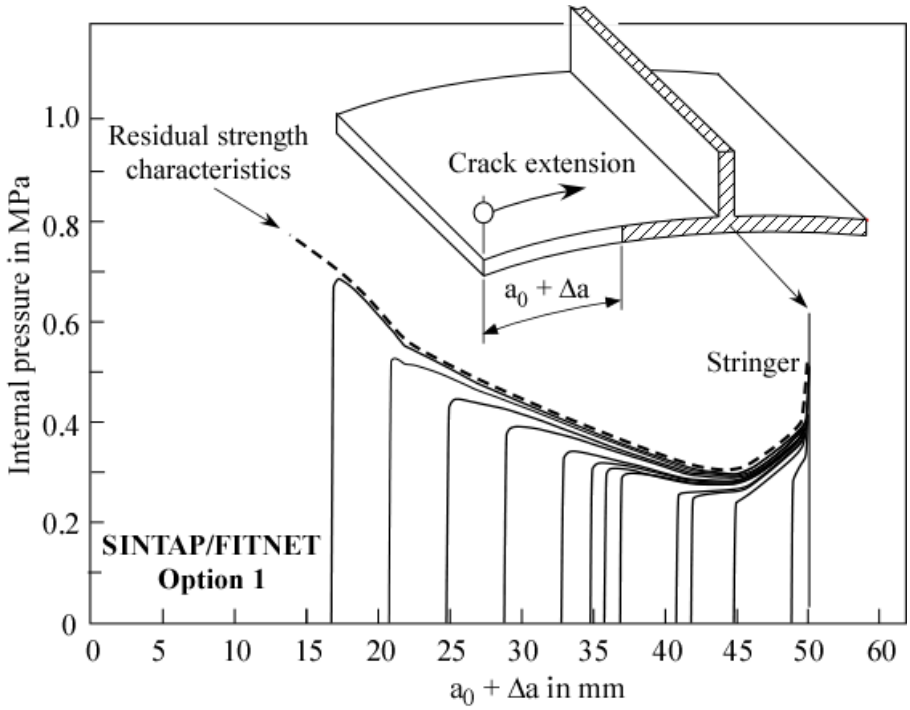

Figure 24: SINTAP/FITNET analysis of a curved stiffened structure using a hybrid approach which combines the analytical methodology with K factor and yield load solutions determined by finite elements (after [111]).

A straightforward approach of structural assessment is the use of the CTOA-δ_5 parameter in finite element analyses. When two nodes of the mesh are positioned 2.5 mm above and below the original crack tip, the δ_5 simply refers to the relative displacement of these nodes. An example for such an analysis is provided in Figure 25 ([81]). Note that a sudden load drop due to the failure of a rivet close to the crack tip caused component failure in this special case. Consequently, the residual strength referred to the intersection of the failure envelope of the rivet with the load vs. δ_5 curve.

A factor which is usually not taken into account is the loading history prior to failure. For example, real in-service conditions are characterized by pre-fatigue loading at relatively high amplitudes compared to the subsequent failure load. This is quite different to laboratory test conditions [81].

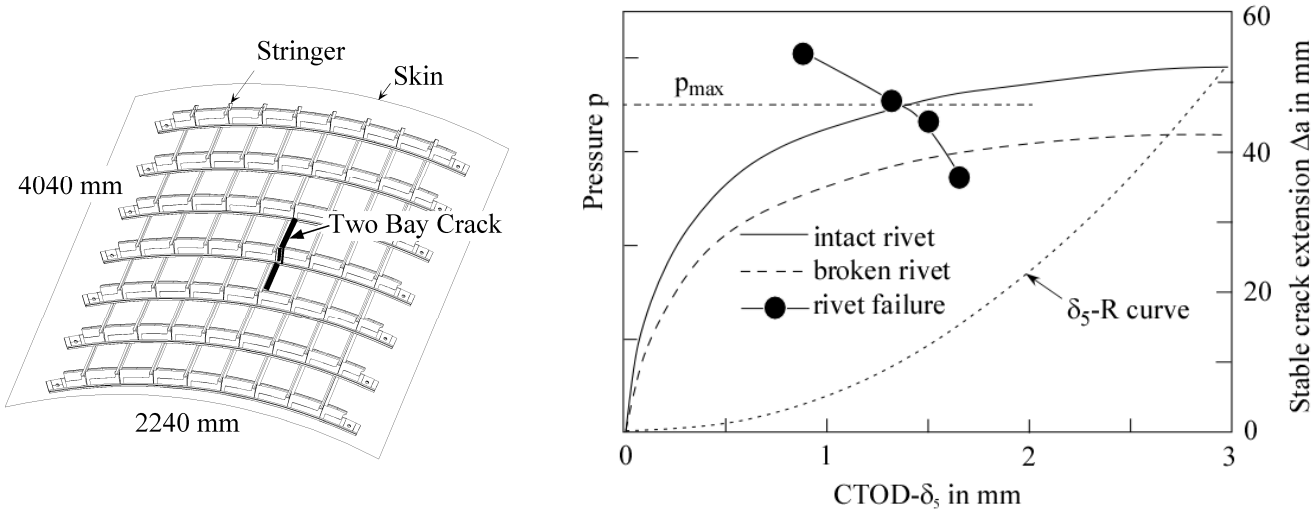

Figure 25: Fuselage panel containing a two-bay crack (left) and residual strength determination based on a finite element δ_5-R-curve approach (after [81], Figure taken from [112]).

3.3 Application of the CTOA, Cohesive Zone and Damage Model Approaches to Panels and Stiffened Shell Structures

CTOA applications to wide plates and component like specimens are presented in [35-36] in this issue and in many other references (e.g. [115-118]), applications of the cohesive model, frequently combined with investigations of the CTOA concept are found in [71] in this issue and elsewhere (e.g. [74, 113, 114, 119]). Note that this list is by no means complete.

An example is shown in Figure 26 where a cylindrical shell with circumferential internal stiffeners containing an axial crack is loaded by internal pressure. The finite element model consisted in a 60º section of the total shell and accounted for symmetry. What is shown is a comparison between the CTOA and cohesive model predictions. Note that both predictions were realized by using different finite element codes.

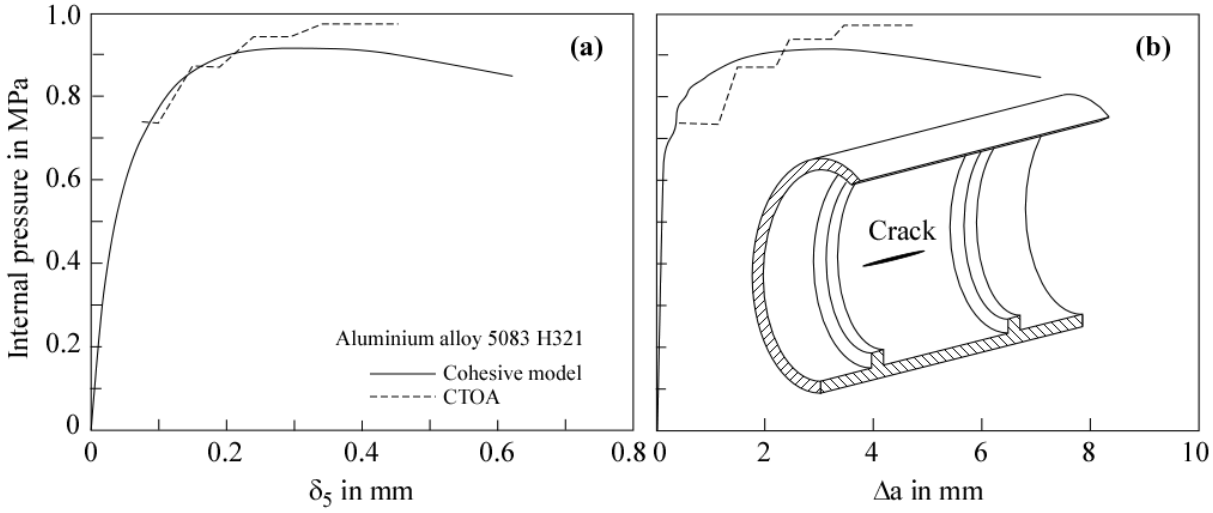

Figure 26: Stiffened cylinder with crack: Prediction of the internal pressure versus δ_5 and Δa characteristics by the CTOA and cohesive models (after [113] and [114]).

A characteristic question in the context of finite element analyses covers the potential mesh dependency of the results. This is even more an issue when the softening behavior of the material has to be simulated. In [114], the authors investigated mesh effects of both the CTOA and the cohesive zone approach. No pathological mesh dependency is expected for the CTOA due to the fact that conventional elasto-plastic constitutive equations are applied. The results are expected to converge with decreasing element size. In Figure 27a no difference was found for two different element sizes (ES). However, the results are affected by the base length (BL) for calculating the CTOA (Figure 27b) but the effect on the maximum load - as the relevant assessment parameter - is small. In Figure 27c it is shown that the mesh dependency of the cohesive zone model is also rather moderate, using a model inherent length scale parameter discussed by Brocks in [120].

A further aspect, which already has been mentioned in Paragraph 2.3, is diverse cohesive zone parameter sets T_0, δ_0 and Γ_0 for two- and three-dimensional analyses which are not interchangeable. Therefore, special care has to be exercised when literature data have to be used.

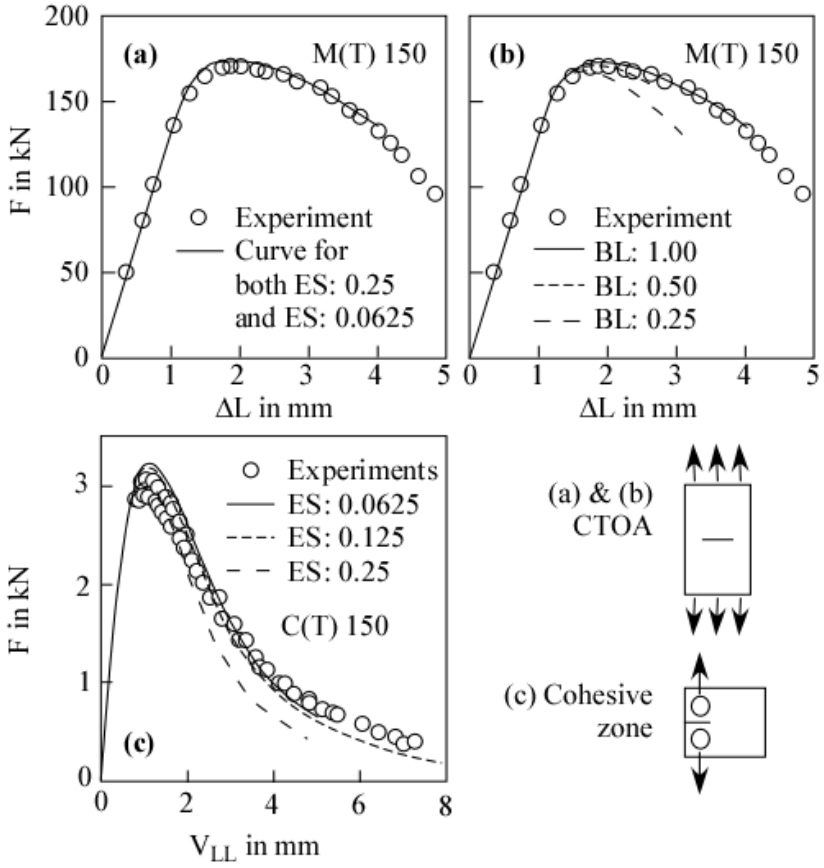

Figure 27: Mesh dependency of CTOA and cohesive zone results. (a) CTOA: element size (ES); (b) CTOA: base length (BL); (c) Cohesive zone: element size (ES).

The application of a GTN (Gurson-Tvergaard-Needleman) type damage model to a thin-walled space structure is presented by Windisch et al. [121] in this issue.

3.4 Specific Aspects of Non-integral and Integral Thin-walled Structures

3.4.1 New Design and Manufacturing Techniques

So far the basic concepts of damage tolerance analyses and their application to simple panel geometries as well as to stiffened and curved shells have been addressed. However, modern developments in design and manufacturing provide additional challenges for the assessment tools. For aircraft applications, these challenges comprise [8,122]:

- the use of new materials and material compounds (e.g., advanced aluminium alloys, e.g. Al-Li or Al-Mg-Sc), CFK, GLARE® etc.,
- innovative structural concepts such as integral components (large extrusions, forgings or castings), hybrid metallic/composite structures etc., and
- innovative joining techniques such as laser and electronic beam and friction stir welding, age creep forming, adhesive and diffusion bonding etc.

Not all these aspects shall be addressed within this paper and the following remarks are a only a partial list rather than a comprehensive summary. The points to be addressed below are multi-site or widespread damage, crack branching and kinking, crack path deviation and problems such as residual stresses and strength mismatch mainly in the context of modern joining techniques.

3.4.2 Multi-site Damage (Widespread Damage)

Multi-site or widespread damage (MSD) became a topic after the Aloha Airlines accident in 1988 [123]. Typically in riveted structures, small cracks can form almost simultaneously at some rivet holes due to high local stresses, corrosion or fretting fatigue [124] (Figure 28). These cracks may grow sub-critically (Figure 29) until they suddenly coalesce to a very long crack with the consequence of dramatic reduction in the component's residual strength. Note that the problem of multi-site damage is not restricted to riveted plates and aircraft components but is also present in other thin wall applications, e.g. pipelines [125-126].

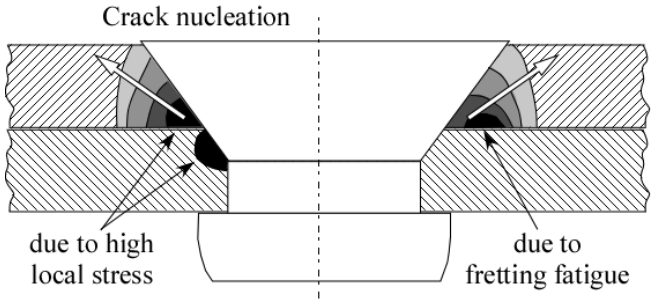

Figure 28: Crack nucleation at a rivet due to high local stresses and fretting fatigue (after [124]).

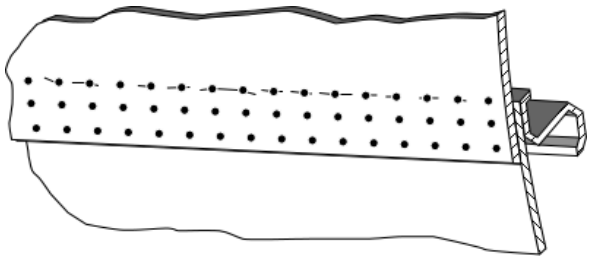

Figure 29: Illustration of multi-site damage in a riveted lap joint.

Reviews on residual strength determination in multi-site damaged components are provided by various authors (e.g. [123, 127]). A number of methods have been proposed for describing the link-up of MSD cracks.

An easy first estimate approach has been proposed by Swift [128] and refined and modified by other authors [129-132]. The basic idea is that the ligament will fail when the plastic zones of two adjacent cracks touch, i.e., the sum of both plastic zones equals the ligament size between the cracks. Various approaches including the K_{eff} concept, the Dugdale model, finite element simulations and semi-empirical fits to test data have been applied to specify the plastic zone sizes. Note that the degree of ligament yielding, L_r, is expected to play a major role with respect to the application ranges of the different approaches. Alternatively the K_R curve model has been applied to multi-site damage, e.g., in [133], sometimes in conjunction with other approaches such as the plastic zone touch criterion mentioned above [134].

Many authors favor the CTOA model for predicting the residual strength of multiple site damaged components [11, 127, 131, 135-138] (for an example see Figure 30). Li and

Siegmund, in [77] showed that the CTOA, instead of being constant, reduces rapidly when the crack tips start to interact and falls even to zero during the link up. That means that the parameter can be used only as long as no interaction between the crack tips takes place which is, however, sufficient for many practical applications.

Only few investigations have been carried out by now on cohesive zone and Gurson type damage modeling of multi-site damage. These are, however, encouraging as Li and Siegmund [77] have shown for the cohesive zone approach and Kim et al. [139] for a modified Gurson approach.

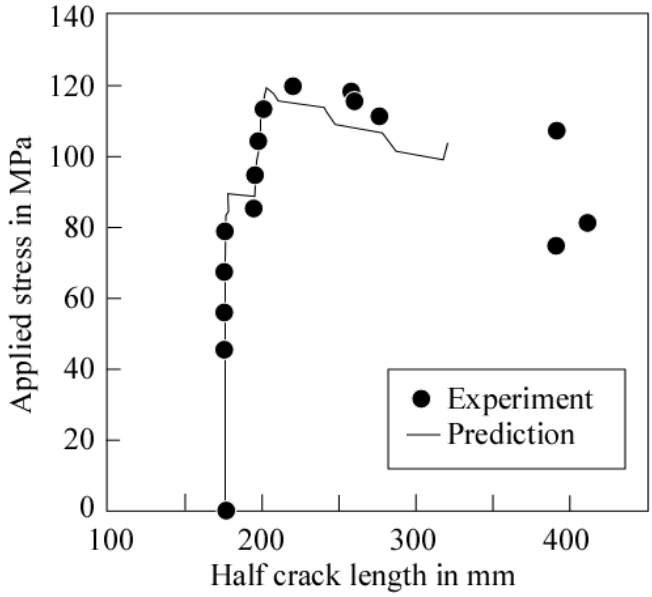

Figure 30: Application of the CTOA criterion to multi-site damage: Comparison between experimental and predicted applied load-stable crack extension characteristics for a flat panel slice joint (see [136]).

3.4.3 Crack Deviation and Branching

While for riveted structures any crack extension is usually restricted to the skin, i.e., the crack grows underneath the stiffener leaving the latter intact, the situation is quite different in integral structures. Figure 31 illustrates the alternative crack growth options of an original skin crack. It can grow underneath the stiffener (path 1), into the stiffener web (path 2) or along the stiffener root (path 3) and, of course, these can also occur in combination.

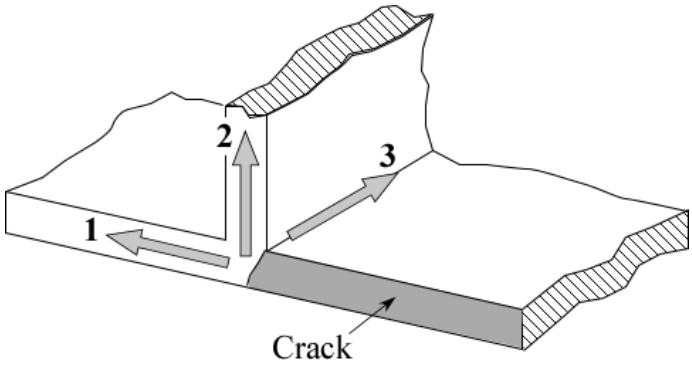

Figure 31: Options of crack extension in an integral structure: Path 1: The crack grows underneath the stiffener; Path 2: It grows into the stiffener web; Path 3: It grows along the stiffener root. In addition combinations of these options are possible.

Common R curve approaches do not, or at least not implicitly, take into account the phenomena of crack path deviation and branching which makes them inappropriate for integral structures. Alternative options are provided by cohesive zone and damage models. It has already been mentioned that the cohesive zone model, by applying specific element configurations, is able to simulate almost arbitrary crack growth directions. However, because a very fine mesh is needed along the potential separation process zones this alternative is limited in practical application. Fortunately there are many cases, including that of Figure 31, where the potential crack paths are known beforehand or can simply be deduced. The fine mesh region may then be restricted to these lines which reduces the effort substantially.

An example is shown in Figure 32 [79]. Investigating the effect of the stiffener thickness on the potential crack path in that special case, the authors found that the crack continued to propagate in its original direction in the skin and additionally into the stiffener when the stiffener thickness was 0.8 mm (Figure 32a). In contrast, for a stiffener thickness of 1.3 mm, the crack deviated and grew in the circumferential direction along the stiffener root, cutting the skin along that line (Figure 32b).

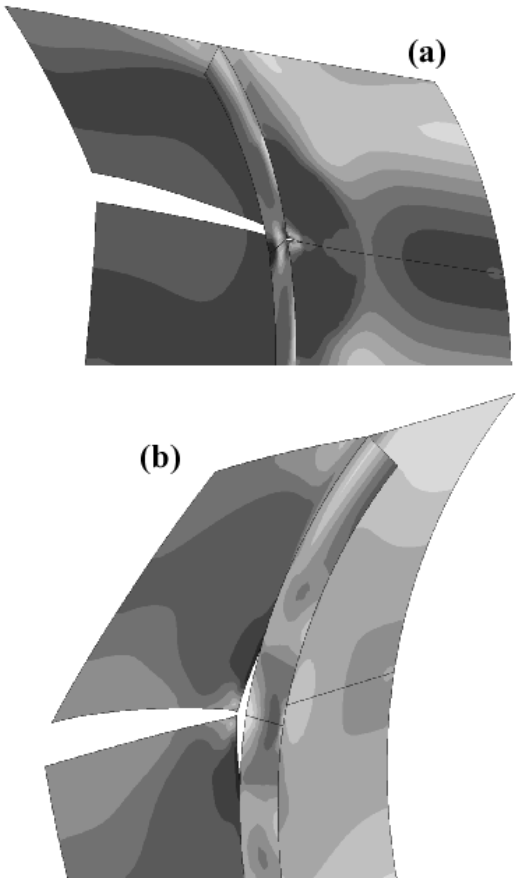

Figure 32: Application of the cohesive zone model to an integral structure consisting of a curved shell (skin) and a circumferential stiffener. (a) For a stiffener thickness of 0.8 mm the crack was found to grow in its original direction in the skin and additionally into the stiffener web; (b) For a stiffener thickness of 1.3 mm the crack deviated and grew circumferentially along the stiffener root (after [79]).

Although crack branching and deviation can also be modeled by damage models, the cohesive zone model is the first choice because its mesh requirements are more moderate, which is of substantial advantage for large components. A simple damage model based on the Rice-Tracey criterion was applied to combined skin and stiffener web crack extension in [140].

3.4.4 Specific Problems of Welded Structures

(a) Welding residual stresses

Integral structures can be large extrusions, forgings, castings etc. but they can also be welded or bonded components. In Figure 33 two types of welds are shown which are used for thin-walled structures made of aluminium. Typical welding technologies for such components are laser beam (LB) or electron beam (EB) welding, variable polarity plasma arc (VPPA) welding and, mainly for butt welds, friction stir welding (FSW) [141]. For steel structures further welding technologies are disposable. Typical damage patterns of weldments of thin walled structures are illustrated in Figure 34.

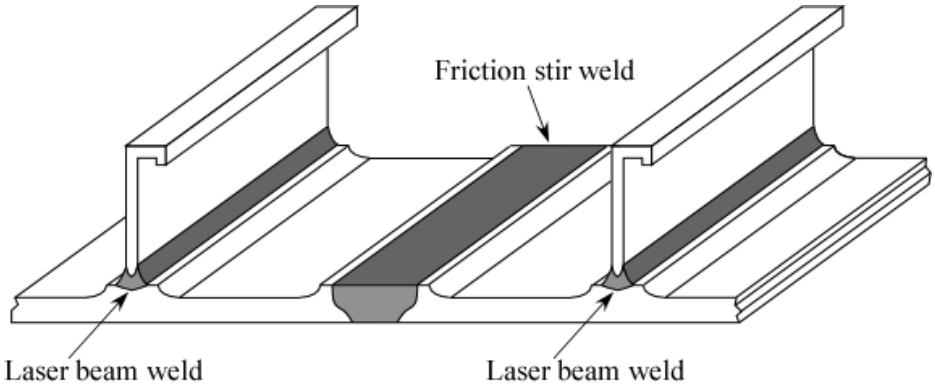

Figure 33: Typical welded structural details in airframes.

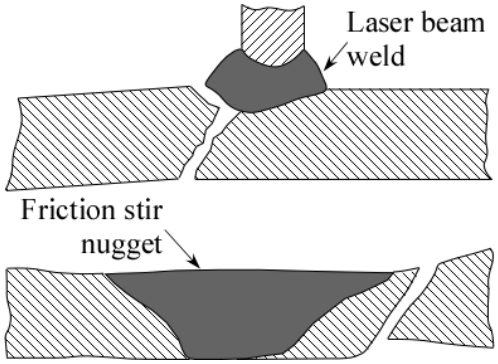

Figure 34: Typical damage patterns in welded thin-walled structures.

For the assessment of welded integral structures specific aspects such as welding residual stresses or strength mismatch have to be taken into account. Two experimental residual stress profiles of a VPPA and a FSW weld are shown in Figure 35.

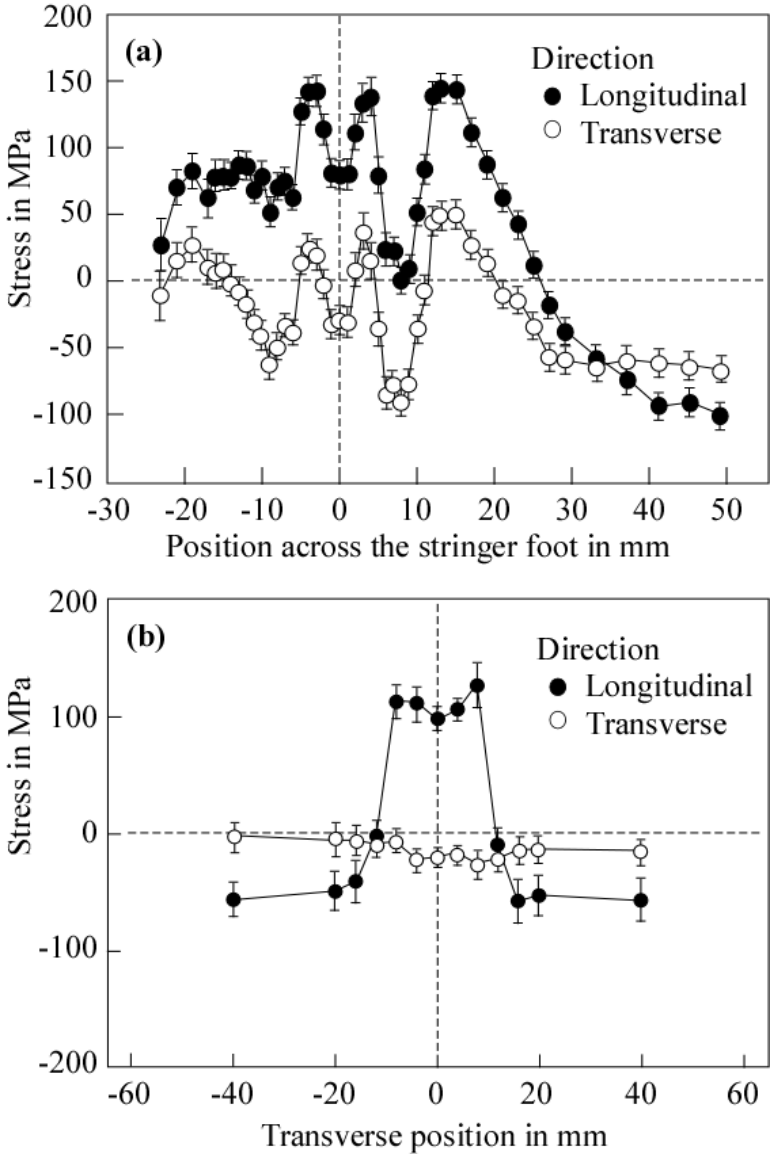

Figure 35: Longitudinal and transverse residual stress profiles (aluminium 2024). (a) along stringer web in a VPPA welded skin-stringer panel (after [142]); (b) in transverse direction of an FSW weld (after [143]).

Welding residual stresses can significantly affect the crack driving force. Its treatment in fracture mechanics is a rather complex issue in most cases. Note, that welding residual stresses are usually classified as secondary stresses in contrast to the primary stresses from the applied loading including inertia effects, dead loading etc. In the frame of a SINTAP/FITNET analysis, such as introduced in Paragraph 3.2, secondary stresses contribute to the K factor but not to the yield load or the L_r parameter respectively.

For small-scale yielding conditions the mode-I stress intensity factor can simply be determined by

$$K_I = K_I^p + K_I^s \tag{18}$$

with the indices “p” and “s” indicating “primary” and “secondary”. However, for contained and net section yielding the situation is more complex. Due to plasticity and relaxation effects the resulting K factor does no longer equal the sum of K_I^p and K_I^s. As a consequence an additional correction term V has to be applied following a concept originally introduced in [144]. Eq. (14) is then re-written as

$$\delta_5 = \frac{1}{\sigma_Y \cdot E'} \cdot \left[\frac{K_I^p + V \cdot K_I^s}{f(L_r)} \right]^2 . \tag{19}$$

where $E' = E$ in plane stress and $E' = E/(1-\nu^2)$ in plane strain or axisymmetry.

The magnitude of the V term mainly depends on the magnitude of the primary and secondary stresses, on the crack size and on the ligament yielding L_r. The latter effect is schematically illustrated in Figure 36. In the contained yielding range approximately up to $L_r = 1$, the plasticity corrected K, i.e., the real crack driving force is larger than $K_I = K_I^p + K_I^s$ because of ligament yielding effects and therefore V > 1. Beyond this range the plasticity corrected K becomes smaller than $K_I^p + K_I^s$ due to relaxation effects. Note that there is a wide range where both effects compete.

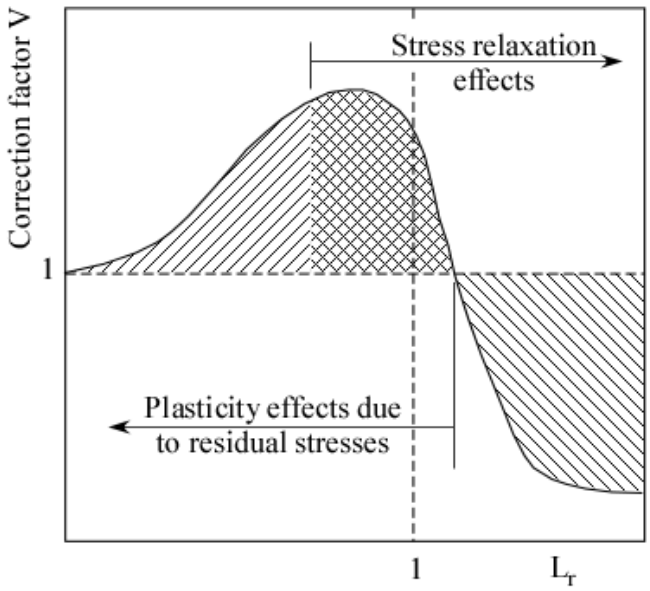

Figure 36: The V correction term as a function of the ligament yielding parameter L_r (schematic).

The V term has been obtained by theoretical analyses backed up by the results of finite analyses. Within assessment procedures such as R6 [107], BS 7910 [108] and SINTAP/FITNET [1, 109] it can be determined by

$$V = \frac{K_p^s}{K_I^s} \cdot \xi \tag{20}$$

with K_I^s being the mode I stress intensity factor due the secondary stresses, K_p^s a plasticity corrected value of K_I^s and ξ an auxiliary function provided in tables. Various approaches exist for determining K_p^s, the easiest of which is based on an effective plastic zone size corrected crack length a_{eff}. (Eq. 4):

$$K_p^s(a) = \left[\frac{a_{eff}}{a}\right]^{1/2} \cdot K_I^s(a). \tag{21}$$

(b) Strength mismatch

Strength mismatch means that material sections of different strength are joined together (e.g. bi-materials or weldments). Common practice is overmatching (OM, the weld is of higher strength than the base metal). The aim is to protect the weld metal from high deformations this way reducing the risk of failure from the weld defects. Typical overmatching ratios are in the order of 10 - 30%, however, in power beam welds they may be as high as 300%. Likewise undermatching applications (UM, the weld is of lower strength than the base metal) exist in thin-walled components, e.g., in joints of aluminium alloys or in joints of very high strength steels. Furthermore, unintentional undermatching may occur, e.g., when the base plate in reality is of much higher strength than required by the manufacturer's specification. In Figure 37 two micro hardness profiles of strength mismatch components are shown for illustration.

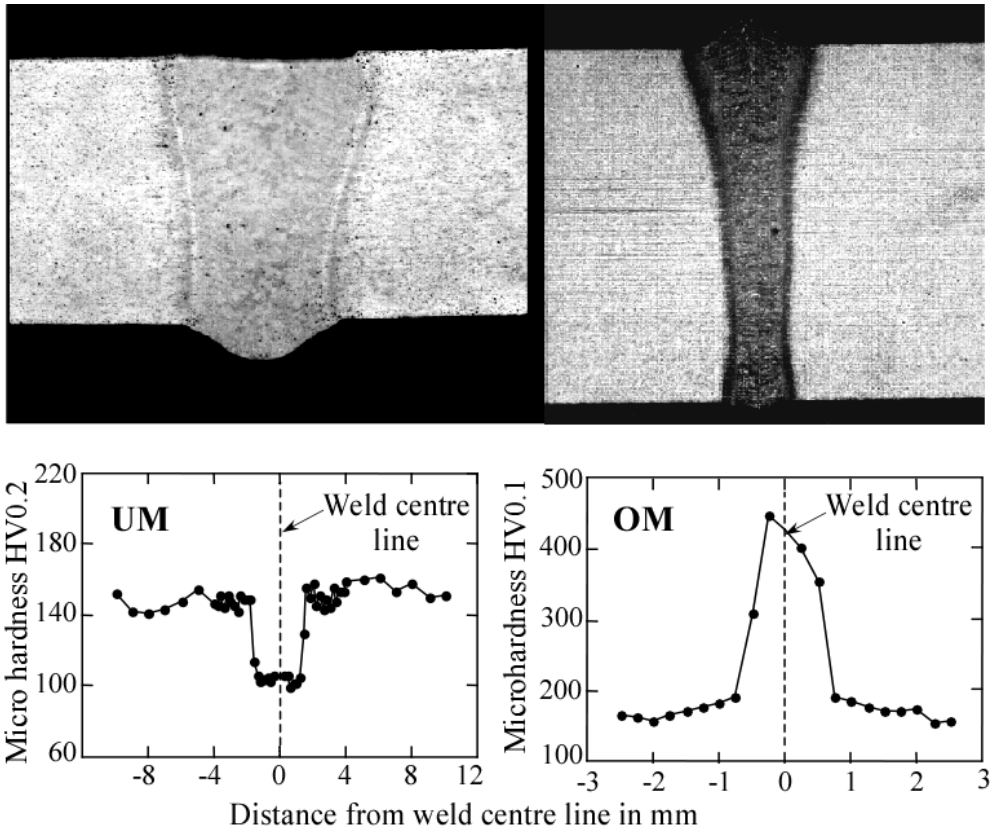

Figure 37: Micro hardness profiles of laser beam welds (a) aluminium alloy, (undermatching); (b) ferritic steel (overmatching) (after [145] and [146]).

The question whether overmatching (or undermatching) is beneficial for structural integrity depends on factors such as the crack location with respect to the weld and on the toughness of the weld and the adjacent material. In general, unfavorable combinations are cracks in the weld center line in undermatched weldments and cracks near the fusion line (e.g., in the heat affected zone) in overmatched weldments.

Depending on the yield strength mismatch ratio M

$$M = \sigma_{YW} / \sigma_{YB} \tag{22}$$

with σ_{YW} being the yield strength of the weld metal and σ_{YB} that of the base material, the strain hardening exponents of the two materials, the component and weld geometry and dimensions and the crack size, shape and location with respect to the weld, various deformation patterns may develop such as illustrated in Figure 38 [147]. Sometimes an existing crack is shielded and a new crack initiates away from the tip, e.g., at the fusion line.

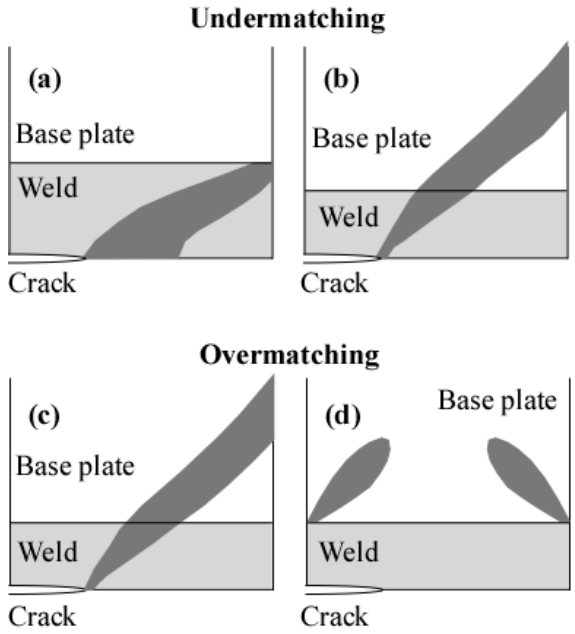

Figure 38: Yield patterns for strength mismatched plates [147]; (a) Undermatching, deformation confined to weld metal; (b) Undermatching, deformation penetrating to the base plate; (c) Overmatching, deformation penetrating to the base plate; (d) Overmatching, base plate deformation.

The mismatch yield pattern affects the overall deformation behavior of the component which is different from both the base material and the weld material components. Within SINTAP/FITNET this effect is taken into account by replacing the base material yield load, F_{YB}, or the weld metal yield load, F_{YW}, by an equivalent mismatch yield load F_{YM}. Solutions of F_{YM} are provided in compendia in various documents [107, 109, 147]. No detailed description of a strength mismatch analysis shall be given here. Instead the reader is referred to [1]. A thin wall strength mismatch example is provided in [148].

Note that the analytical SINTAP/FITNET assessment of strength mismatch components is restricted to applications for which F_{YM} solutions are available. Up to now, these comprise only butt welds. Damage models can be applied much more flexible to mismatch problems.

An example is provided in Figure 39 where crack extension in a laser beam welded 6000 series aluminium sheet has been simulated [149]. Crack path deviation from the weld line towards the softer fusion zone, such as experimentally observed, was predicted by the 3D damage model.

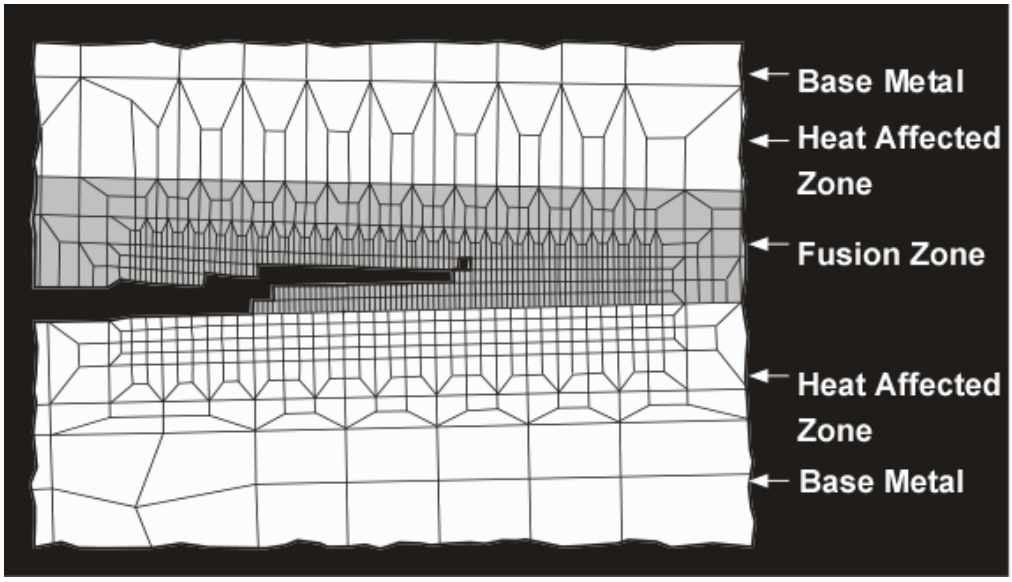

Figure 39: Prediction of crack path kinking of a heat affected zone crack into the fusion zone of a laser welded aluminium alloy sheet by a damage mechanics model [149, 150].

3.4.5 Specific Problems of Bonded Structures

The use of bonded construction, particularly for aerospace applications, has a long history [151]. In many applications the use of bonded structures was chosen based on manufacturing preferences, the potential damage tolerance benefit of bonded construction has been realized and documented [152]. Conventional linear elastic fracture mechanics has successfully been applied to bonded skin-stiffener connections, particularly for fuselage applications [153]. One application of bonded structures that has received significant attention in the last 15 years is the use of bonded patches to repair aging aircraft structures [154-155]. Analysis of these types of structures consisted of applying the cyclic linear elastic stress intensity factor concept to crack growing in the metallic structure, including a correction to account for the crack bridging effect from the bonded stiffeners or repair patches. Besides the K factor concept the cohesive zone approach is gaining in importance for describing damage of bonded structures. Some recent applications to thin-walled structures are provided in [156-158].

Recently a new concept of using bonded structures to enhance the damage tolerance of aircraft structures *ab initio* has been introduced and studied [159-161]. The article by Zhang and Irving in this special issue [162] provides additional information on analysis approaches for damage tolerance assessments for structures with bonds or stiffeners. The work in the above cited references also indicates the importance of incorporating residual stress effects and the delamination growth behavior in the analysis models. Residual stresses are generated in bonded structures during the typical autoclave bond cycle as a result of mismatch in thermal expansion coefficient between the metallic substrate and the applied reinforcement material. Heinimann [159] showed the impact residual stress effects have on fatigue crack

growth performance by testing aluminum plate reinforced with a carbon-epoxy fiber metal laminate, that was bonded in two different ways, thus generating test panels that had either very little or significant bond cycle induced residual stress (Figure 40).

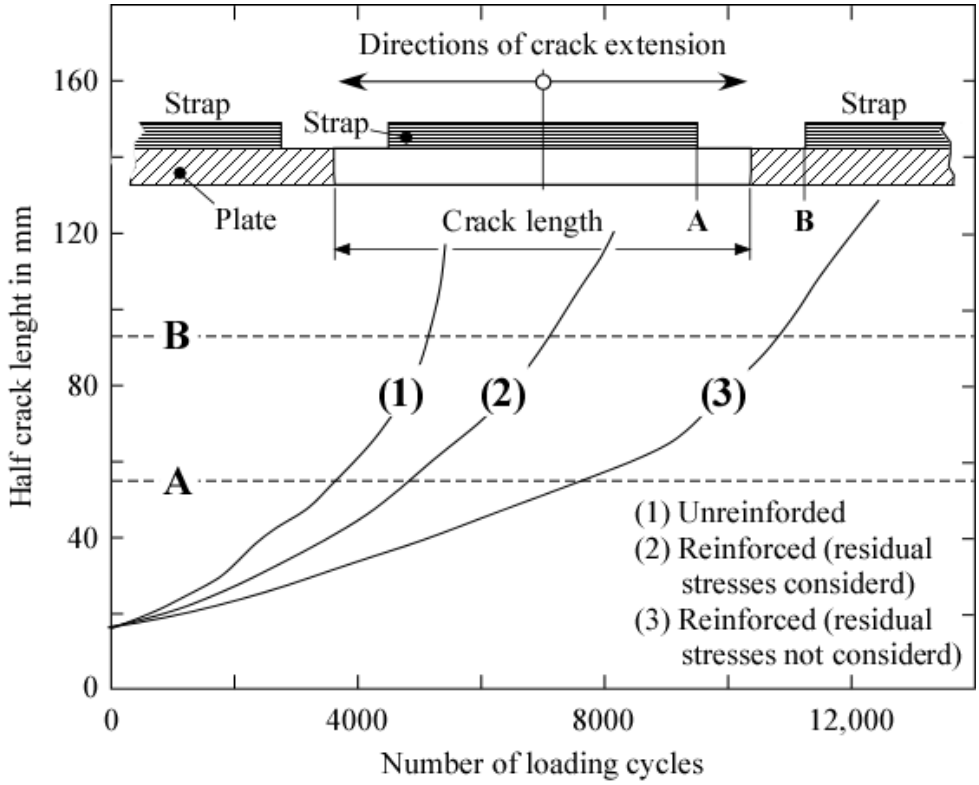

Figure 40: Experimental crack extension curves for flat panels with reinforcement, highlighting the effect of bond cycle induced residual stresses [159].

Note that the delamination models described above only consider the development and extension of the delamination. However, for structural integrity assessment, the combination of crack propagation in the metal structure and associated delamination growth at the interface needs to be considered. This problem is also very similar to the damage progression in fiber metal laminate (FML) structures [163-164]. The remarkable damage tolerance capability of FML and selectively reinforced structures are attributable to load distribution and crack bridging that occurs in these multi layer and multi-material structures. Figure 41 schematically shows the load redistribution from the cracked metal outer layers to the intact fiber layer in a basic FML. In order to understand and predict the damage tolerance behavior of FML or selectively reinforced structures, all of the relevant failure modes, including, crack propagation in the metallic layers and delamination growth at interface and within the fiber and adhesive layers need to be considered.

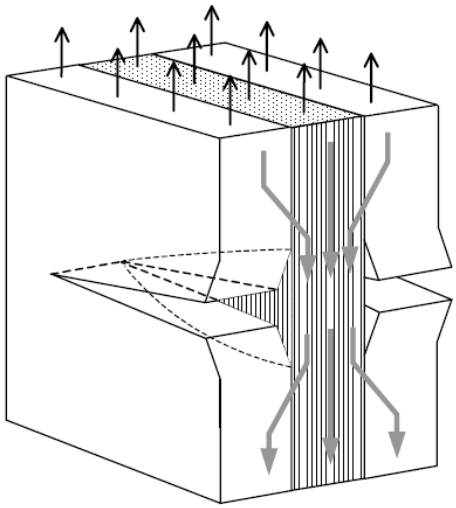

Figure 41: Schematic showing load redistribution and crack bridging in an FML (Figure after [163]).

4. SUMMARY

This paper reviews the most important current approaches for residual strength prediction of thin-walled structures. Crack driving force parameters such the linear elastic stress intensity factor and its plastic zone corrected extension for contained yielding conditions, the crack tip opening displacement δ_5, the crack tip opening angle CTOA, the cohesive zone model parameters, separation energy, critical tensile stress and critical separation and the parameters of the damage models of Gurson-Tvergaard-Needleman type are introduced and discussed with respect to their benefits and limitations for the simulation of plane and stiffened panels. In addition, specific aspects of modern non-integral and integral structures which pose a challenge are addressed. These comprise multi-site damage, crack deviation and branching, welding residual stresses, strength mismatch in material compounds and problems in bonded structures, such as delamination. A number of examples are provided to illustrate the potential of the various approaches. Further discussion and case studies are presented in the papers within this issue.

References

[1] Zerbst, U., Schödel, M., Webster, S. and Ainsworth, R.A. (2007): Fitness-for-Service Fracture Assessment of Structures Containing Cracks. A Workbook based on the European SINTAP/FITNET Procedure. Elsevier.

[2] Weitzman, R.H. and Finnie, I. (1972): Measuring fracture toughness – a simplified approach using controlled crack propagation. J. Mat. 7, 294-299.

[3] ASTM E 399-90 (re-approved 1997): Standard Test Method for Plane-Strain Fracture Toughness of Metallic Materials. ASTM International.

[4] NASGRO 3.0 (2000): Fatigue Crack Growth Computer Program “NASGRO” Version 3.0. National Aeronautics and Space Administration, Lyndon B. Johnson Space Centre, Houston, Texas.

[5] USAF Handbook for Damage Tolerant Design, Last update 2002, Chapter 4.5: Residual Strength. Built-up structures.

[6] Poe, C.C., Jr. (1971): Stress-intensity factor for a cracked sheet with riveted and uniformly spaced stringers. NASA Technical Report TR R-358.

[7] Rooke, D.P. and Cartwright, D.J. (1974): Compendium of Stress Intensity Factors. HMSO, London, Chapter 2: Stiffened Sheets.

[8] Schmidt, H.-J. (1995): Damage tolerance technology for current and future aircraft structure. Proc. 23rd ICAF Symposium of the Int. Committee on Aeronautical Fatigue, Hamburg, Germany, Plantema Memorial Lecture, Vol. 1, 1-41.

[9] Toor, P.M. (1986): On damage tolerance design of fuselage structure (longitudinal cracks. Engng. Fracture Mech. 24, 915-927.

[10] Toor, P.M. (1987): On damage tolerance design of fuselage structure - circumferential cracks. Engng. Fracture Mech. 26, 771-782.

[11] Newman, J.C., Jr. (1999): Advances in fatigue and fracture mechanics analyses for aircraft structures. Proc. 20th ICAF Symposium of the Int. Committee on Aeronautical Fatigue, Bellevue, Washington, Plantema Memorial Lecture, 3-42.

[12] Ingraffea, A.R. and Wawrzynek, P.A. (2003): Finite element method for linear elastic fracture mechanics. In: de Borst, R. and Mang, H.A. (eds.): Comprehensive Structural Integrity, Vol. 3: Numerical and Computational Methods. Elsevier, Amsterdam et al., 1-88.

[13] Aliabadi, M.H. (2003): Boundary element methods in linear elastic fracture mechanics. In: de Borst, R. and Mang, H.A. (eds.): Comprehensive Structural Integrity, Vol. 3: Numerical and Computational Methods. Elsevier, Amsterdam et al., 891-125.

[14] Atkins, A.G. (2003): Thin sheet fracture. In: Milne, I., Ricthie, R.O. and Karihaloo, B.: Comprehensive Structural Integrity. Vol. 1: Structural Integrity Assessment. Chapter 1.17, 355-376.

[15] Margolis, W.S. and Nordquist, F.C. (1975): Plane stress fracture toughness (K_c) of aluminium alloy 7475-1/2 inch plate, tempers-T7651 and T7351 and of aluminium alloy 2024-1/8 inch sheet-T81 and T62 temper. General Dynamics, Fort Worth Div., F-16 Air Combat Fighter Technical Reports TIS GA2300, CDRL A031,
USAF Contract F33657-75-C-0310.

[16] Krafft, J.M., Sullivan, A.M. and Boyle, R.W. (1961): Effect of dimensions on fast fracture instability of notched sheets. In: Kennedy, A.J. (ed.): Proc. of Symposium on Crack Propagation, Cranfield, U.K., 8-28.

[17] McCabe, D.E. (ed.) (1973): Fracture Toughness Evaluation by the R-Curve Method. ASTM STP 527.

[18] ASTM E 561-98 (1998): Standard Practice for R-Curve Determination. ASTM International. West Conshohocken, PA.

[19] Anderson, T.L. (1991): Fracture Mechanics. CRC Press Inc., Boca Raton, Florida.

[20] Schwalbe K.-H., Heerens, J., Zerbst, U., Pisarski, H. and Koçak, M. (2002): EFAM-GTP 02. The GKSS Procedure for Determining the Fracture Behavior of Materials. GKSS-Research Centre Geesthacht. GKSS Report 2002/24.

[21] ESIS P3-04D (2007): Draft Unified Procedure for Determining the Fracture Behavior of Material. European Structural Integrity Society (ESIS).

[22] Schwalbe, K.H-, Newman, J.C., Jr. and Shannon, J.L. Jr. (2005): Fracture mechanics testing on specimens with low constraint—standardization activities within ISO and ASTM. Engng. Fracture Mech. 72, 557-576.

[23] Concalves, W., Pramono, A. and Chaves, C.E. (2004): Embraer new family of jets – meeting the current fatigue and damage tolerance requirements. Proc. 22th ICAF Symposium of the Int. Committee on Aeronautical Fatigue, Sheffield, U.K., 231-257.

[24] Ehrström, J.C. (2007): Utilization of K_{eff} based R-curves in the case of extended plastic yielding. This issue, xxx-xxx.

[25] ASTM E 1820-01 (2001): Standard Test Method for Fracture Toughness. ASTM International. West Conshohocken, PA.

[26] ISO 12135 (2003): Metallic Materials – Unified Method of Test for the Determination of Quasistatic Fracture Toughness. International Standard Organisation (ISO).

[27] Schwalbe, K.-H. (1995): Introduction of δ_5 as an operational definition of the CTOD and its practical use. ASTM STP 1256, 763-78. American Society for Testing and Materials.

[28] Schwalbe, K.-H. and Heerens, J. (1998): R-curve testing and its relevance to structural assessment. Fatigue Fracture Engng. Mat. Structures 21, 1259-1271.

[29] Anderson, H. (1973): Finite element representation of stable crack growth. J. Mech. Phys. Solids 21, 337-356.

[30] de Koning, A.U. (1977): A contribution to the analysis of quasi static crack growth in steel materials. In: Fracture 1977, Proc. 4th Int. Conf. Fracture (ICF4), Vol. 3, 25-31.

[31] Demofonti, G. and Rizzi, L. (1991): Experimental evaluation of CTOA in controlling unstable ductile fracture propagation. In: Blauel, J.G. and Schwalbe, K.-H. (eds.): Defect Assessment in Components – Fundamentals and Applications, SEIS/EGF 9, Mech. Engng. Publ., London, 693-703.

[32] Newman, J.C., Jr., Dawicke, D.S. and Bigelow, C.A. (1992): Finite element analysis and measurement of CTOA ductile stable tearing in a thin sheet aluminium alloy. Proc. Int. Workshop on Structural Integrity of Aging Airplanes. Atlanta, Georgia, 167-186.

[33] Kanninen, M.F., Popelar,, C.H. and Broek, D. (1981): A critical survey on the application of plastic fracture mechanics to nuclear pressure vessels and piping. Nuclear Engng. and Design 67, 27-55.

[34] Newman, J.C., Jr. and Zerbst, U. (eds.) (2003): Special Issue on Fundamentals and Applications of the Crack Tip Opening Angle (CTOA). Engng. Fracture Mech. 70, Numbers 3-4, 367-577.

[35] James, M. and Bucci, B. (2007) Resistance curve predictions using the constant CTOA toughness fracture criterion. Engng. Fracture Mech., This issue, xxx-xxx.

[36] Pirondi, A. and Fersini, D. (2007): Simulation of ductile crack growth in thin panels using CTOA. Engng. Fracture Mech., This issue, xxx-xxx.

[37] Heerens, J., Schödel, M. and Schwalbe, K.-H. (2007): Determination of the critical crack tip opening angle CTOA using the CTOD-δ_5 measurement technique. Engng. Fracture Mech., This issue, xxx-xxx.

[38] Newman, J.C., Jr., James, M.A. and Zerbst, U. (2003): A review of the CTOA/CTOD fracture criterion. Engng. Fracture Mech. 70, 371-385.

[39] Dawicke, D.S. and Sutton, M.A. (1994): CTOA and crack tip tunneling measurements in aluminium alloy 2024-T3. Exp. Mech. 34, 357-368.

[40] Heeerens, J. and Schödel, M. (2003): On the determination of crack tip opening angle, CTOA, using light microscopy and δ_5 measuring technique. Engng. Fracture Mech. 70, 417-426.

[41] Sutton, M.A., Turner, J.L., Bruck, H.A. and Chae, T.A. (1991): Full-field representation of discretely sampled surface deformation for displacement and strain analysis. Exp. Mech. 31, 168-177.

[42] Dawicke, D.S., Newman, J.C., Jr. and Bigelow, C.A. (1995): Three-dimensional CTOA and constraint effects during stable tearing in a thin-sheet material. ASTM STP 1256, 223-242.

[43] Ma, L., Lam, P.W. Kokaly, M.T. and Kobayashi, A.S. (2003): CTOA of a stable crack in a thin aluminium fracture specimen. Engng. Fracture Mech. 70, 427-442.

[44] Shterenlikht, A., Hashemi, S.H., Howard, I.C., Yates, J.R. and Andrews. R.M. (2004): A specimen for studying the resistance to ductile crack propagation in pipes. Engng. Fracture Mech. 71, 1997-2013.

[45] Lloyd, W.R. (2003): Microtopography for ductile fracture process characterization. Part 1: Theory and methodology. Engng. Fracture Mech. 70, 387-401.

[46] Lloyd, W.R. and McClintock (2003): Microtopography for ductile fracture process characterization. Part 2: Application for CTOA analysis. Engng. Fracture Mech. 70, 403-415.

[47] Shivakumar, K.N. and Newman, J.C., Jr. (1990): ZIP3D – An elastic-plastic finite-element analysis program for cracked bodies. NASA TM 102753.

[48] Hampton, R.W. and Nelson, D. (2003): Stable crack growth and instability prediction in thin plates and cylinders. Engng. Fracture Mech. 70, 469-491.

[49] Mahmoud, S. and Lease, K. (2004): Two-dimensional and three dimensional finite element analyses of critical crack-tip-opening angle in 2024-T351 aluminium alloy at four thicknesses. Engng. Fracture Mech. 71, 1379-1391.

[50] Newman, J.C., Jr., Dawicke, D.S. and Seshadri, B.R. (2003): Residual strength analyses of stiffened and un-stiffened panels – Part I: laboratory specimens. Engng. Fracture Mech. 70, 493-507.

[51] Demofonti G, Buzzichelli, G., Venzi, S. and Kanninen, M. (1995): Step by step procedure for the two specimen CTOA test. In: Denys, R. (ed.): 3rd. Int. Pipeline conference, Brugge, Belgium, Vol. II, 503-12.

[52] Salvini, P., Fonzo, A. and Mannucci, G. (2003): Identification of CTOA and fracture process parameters by drop weight test and finite element simulation. Engng. Fracture Mech. 70, 553-566.

[53] Rudland, D.L., Wilkowski, G.M., Feng, Z., Wang, Y.-Y., Horsley, D. and Glover, G. (2003): Experimental investigation of CTOA in linepipe steels. Engng. Fracture Mech. 70, 567-577.

[54] Mahmoud, S. and Lease, K. (2003): The effect of specimen thickness on the experimental characterization of critical crack-tip-opening angle in 2024-T351 aluminium alloy. Engng. Fracture Mech. 70, 443-456.

[55] Dawicke, D.S., Newman, J.C., Jr., Starnes, J.H., Jr., Rose, C.A., Youn, R.D. and Seshardy, B.R. (1999): Residual strength analysis methodology: Laboratory coupons to structural components. Third Joint FAA/DoD/NASA Conf. on Aging Aircraft. Albuquerque, MN.

[56] Mahmoud, S. and Lease, K. (2004): Two-dimensional and three dimensional finite element analyses of critical crack-tip-opening angle in 2024-T351 aluminium alloy at four thicknesses. Engng. Fracture Mech. 71, 1379-1391.

[57] Newman, J.C., Jr., Crews, J.H., Jr., Bigelow, C.A and Dawicke, D.S (1995): Variations of the global constraint factor in cracked bodies under tension and bending loads. ASTM STP 1244, 21-42.

[58] Brocks, W., Eberle, A. Fricke, S. and Veith, H. (1994): Large stable crack growth in fracture mechanics specimens. Nuclear Engng. Design 151, 387-400.

[59] James, M.A. and Newman, J.C., Jr. (2002): Three-dimensional analyses of crack-tip-opening angles and δ_5-resistance curves for 2024-T351 aluminium alloy. ASTM STP 1406, 279-297.

[60] James, M.A. and Newman, J.C., Jr. (2003): The effect of crack tunneling on crack growth: experiments and CTOA analyses. Engng. Fracture Mech. 70, 457-468.

[61] Schödel, M. and Zerbst, U. (2004): Application of the European flaw assessment procedure SINTAP to thin wall structures. Analytical assessment levels. Engng. Fracture Mech. 71, 1035-1058.

[62] Dugdale, D.S. (1960): Yielding of steel sheets containing slits. J. Mech. Phys. Solids 8, 100-108

[63] Barenblatt, G.I. (1962): The mathematical theory of equilibrium of cracks in brittle fracture. Adv. Appl. Mech. 7, 55-129.

[64] Needleman, A. (1987): A continuum model for void nucleation by inclusion debonding. J. Appl. Mech. 54, 525-531.

[65] Elices, G.V., Guinea, J., Gomez, J. and Planas, J. (2002): The cohesive zone model: advantages, limitations and challenges. Engng. Fracture Mech. 69, 137-163.

[66] Brocks, W., Cornec, A. and Scheider, I. (2003): Computational aspects of nonlinear fracture mechanics. In: de Borst, R. and Mang, H.A. (ed.): Comprehensive Structural Integrity, Vol. 3: Numerical and computational methods. Elsevier Ltd., 127-209.

[67]: Brocks, W. and Cornec, A. (eds.) (2003): Special Issue on Cohesive Models. Engng. Fracture Mech. 70, Numbers 14, 1741-1987.

[68] Xu, X. and Needleman, A. (1994): Numerical simulations of fast crack growth in brittle solids. J. Mech. Phys. Solids 42, 1397-1434.

[69] Scheider, I. and Brocks, W. (2003): Simulation of cup-cone fracture using the cohesive zone model. Engng. Fracture Mech. 70, 1943-1961.

[70] Cornec, A., Scheider, I. and Schwalbe, K.-H. (2003): On the practical application of the cohesive model. Engng. Fracture Mech. 70, 1963-1987.

[71] Scheider, I. (2007): Residual strength prediction of a complex structure using crack extension analyses. Engng. Fracture Mech., This issue, xxx-xxx.

[72] Nègre, P., Steglich, D. and Brocks, W. (2005): Crack Extension at an Interface: Prediction of Fracture Toughness and Simulation of Crack Path Deviation. Int. J. Fracture 134, 209-229.

[73] Chen, C.R., Kolednik, O., Heeeens, J. and Fischer, F.D. (2005): Three-dimensional modeling of ductile crack growth: Cohesive zone parameters and crack tip triaxiality. Engng. Fracture Mech. 72, 2972-2094.

[74] Roy, Y.D.A. and Dodds, R.H. (2001): Simulation of ductile crack growth in thin aluminium panel using 3-D surface cohesive elements. Int. J. Fracture 110, 21-45.

[75] Roychowdhury, S., Roy, Y.D.A. and Dodds, R.H., Jr. (2002): Ductile tearing in thin aluminium panels: experiments and analyses using large-displacement, 3-D surface cohesive elements. Engng. Fracture Mech. 69, 983-1002.

[76] Lin, G., Cornec, A. and Schwalbe, K.-H. (1998): Three-dimensional finite element simulation of crack extension in aluminium alloy 2024-FC. Fatigue & Fracture of Engng. Mat. & Struct., 21, 1159-1173.

[77] Yuan, H., Lin, G. and Cornec, A. (1996): Verification of a cohesive zone model for ductile fracture. J. Engng. Mater. Techn. 118, 192-200.

[78] Li, W. and Siegmund, T. (2002): An analysis of crack growth in thin-sheet metal via a cohesive zone model. Engng. Fracture Mech. 69, 2073-2093.

[79] Scheider, I. and Brocks, W. (2006): Cohesive elements fort thin-walled structures. Computational Materials Science. 37, 101-109.

[80] Siegmund, T. and Brocks, W. (2000): The role of cohesive strength and separation energy for modeling of ductile fracture. ASTM STP 1360, 139-151.

[81] Cornec, A., Schönfeld, W., Brocks, W. and Assler, H. (2005): Restfestigkeit von Flugzeugrumpfschalen: Finite Element Analyse und Experiment. 37th Symposium of„ K Bruchvorgänge“, Germany, 65-74.

[82] Kachanov, L.M. (1958): On the time to failure under creep conditions. Izv. Akad. Nauk. SSR 8, 26–31.

[83] Beremin, F.M. (1981): Cavity formation from inclusions in ductile fracture of A508 steel. Metall. Trans. 12A, 723–731.

[84] Beremin, F.M. (1983): A local criterion for cleavage fracture of a nuclear pressure vessel steel. Metall. Trans. 14A, 2277–2287.

[85] Lemaitre, J. (1986): Local approach of fracture. Eng. Fracture Mech. 25, 523–527.

[86] Lemaitre, J., (1987): Continuum damage mechanics: theory and applications. Technical Report 295, CISM, Udine.

[87] Rousselier, G. (1987): Ductile fracture models and their potential in local approach of fracture. Nucl. Eng. Design 105, 97–111.

[88] Eshelby, D. (1957): The determination of the elastic field of an ellipsoidal inclusion, and related problems. Proc. Royal Soc. London A 241, 376–396.

[89] Hill, R. (1965): A self-consistent mechanics of composite materials. J. Mech. Phys. Solids 13, 213–222.

[90] Hutchinson, J.W. (1976): Bounds and self-consistent estimates for creep of polycrystalline materials. Proc. Royal Soc. London A 348, 101–127.

[91] Rice, J.R., and Tracey, D.M. (1969): On the ductile enlargement of voids in triaxial stress fields. J. Mech. Phys. Solids 17, 201–217.

[92] Gurson, A. L. (1977). Continuum theory of ductile rupture by void nucleation and growth: Part I - Yield Criteria and Flow Rules for Porous Ductile Media, J. Engng. Materials and Technology 99, 2-15.

[93] Needleman, A., and Tvergaard, V. (1984): An analysis of ductile rupture in notched bars, J. Mech. Phys. Solids 32, 461-490.

[94] Needleman, A., and Tvergaard, V. (1987): An analysis of ductile rupture modes at a crack tip. J. Mech. Phys. Solids 35, 151-183.

[95] Brocks, W., Klingbeil, D., Künecke, G., and Sun, D.-Z. (1995a): Application of the Gurson model to ductile tearing resistance. Second Symposium on Constraint Effects, ASTM STP 1224, 232-252, American Society for Testing and Materials.

[96] Xia, L., and Shih, F.C. (1995): Ductile crack growth - I: A numerical study using computational cells with microstructurally-based length scales, J. Mech. Phys. Solids 43, 223-259.

[97] Ruggieri C., Panontin T.L., and Dodds R.H. (1996): Numerical modeling of ductile crack growth in 3-D using computational cell elements. Int. J. Fracture 82, 1996, 67-95

[98] Sun, D. Z., Hönig, A., Böhme, W., and Schmitt, W. (1994): Application of micromechanical models to the analysis of ductile fracture under dynamic loading. ASTM STP 1220, 343-357. 94, American Society for Testing and Materials.

[99] Nègre, P., Steglich, D., and Brocks, W. (2004): Crack extension in aluminium welds: a numerical approach using the Gurson-Tvergaard-Needleman model, Eng. Fract. Mech., 71, 2365-2383.

[100] Wyart, E., Coulon, D., Pardoen, T., Remacle, J.F. and Lani, F. (2007): Application of the substructured Finite Element / eXtended Finite Element (S-FE/XFE) Method to the analysis of cracks in aircraft thin walled structures. Engng. Fracture Mech., This issue, xxx-xxx.

[101] J. Sumpter (1993): An experimental investigation of the T stress approach, Constraint Effects in Fracture, ASTM STP 1171, 492–502, American Society for Testing and Materials.

[102] A. Pineau (1992): Global and local approaches to fracture – transferability of laboratory test results to components, in: A.S. Argon (Ed.), Topics in Fracture and Fatigue, Springer Verlag Inc., NY, 197-234.

[103] J. Besson, W. Brocks, O. Chabanet, D. Steglich (2001): Ductile rupture of aluminum sheet materials, European Journal of Finite Elements 10, 401-415.

[104] Chabanet, O., Steglich, D., Besson, J., Heitmann, V., Hellmann, D., and Brocks, W. (2003). Predicting crack growth resistance of aluminium sheets. Comp. Mater. Sci. 26, 1-12.

[105] USAF Handbook for Damage Tolerant Design, Last update 2002, Chapter 4: Residual Strength.

[106] Nesterenko, B.G. (2004): Analysis of stiffened structure residual strength using R-curve of skin material. Proc. 22th ICAF Symposium of the Int. Committee on Aeronautical Fatigue, Sheffield, U.K., 749-761.

[107] R6, Revision 4 (2000): Assessment of the Integrity of Structures Containing Defects. British Energy Generation Ltd (BEGL), Barnwood, Gloucester.

[108] BS 7910 (2005): Guide on Methods for Assessing the Acceptability of Flaws in Metallic Structures. British Standard Institution (BSI), London.

[109] Kocak, M., Webster, S., Janosch, J.J., Ainsworth, R.A. and Koers, R. (2006): Fitness for Service Procedure (FITNET), Final Draft 7.

[110] Schödel, M., Zerbst, U. and Dalle Donne, C. (2006): Application of the European flaw assessment procedure SINTAP to thin wall structures subjected to biaxial and mixed mode loadings. Engng. Fracture Mech. 73, 626-642.

[111] Zerbst, U., Schödel, M. and Ata-Ur, R. (2005): unpublished results.

[112] Brocks, W., Schwalbe, K.-H. and Zerbst, U. (2006): Structural integrity assessment of thin-walled structures. Advanced Engng. Mat. 8, 319-327.

[113] Schödel, M., Scheider, I., Iberer, T. and Rother, K. (2005): Residual strength of thin-walled structures based on the CTOA approach of ANSYS. 23rd CAD-FEM Users Meeting.

[114] Brocks, W., Scheider, I. and Schödel, M. (2006): Simulation of crack extension in shell structures and prediction of residual strength. Arch. Appl. Mech. 76, 655-665.

[115] Baumeister, W.J. and Kalal, D.R. (2005): The design and certification of a monolithic spar in a light business jet. Proc. 23rd ICAF Symposium of the Int. Committee on Aeronautical Fatigue, Hamburg, Germany, Vol. I, 177-188.

[116] Seshadri, B.R., Newman, J.C. and Jr., Dawicke, D.S. (2003): Residual strength analyses of stiffened and un-stiffened panels – Part II: wide panels. Engng. Fracture Mech. 70, 493-507.

[117] Baewell, C.A., Eber, L. and Fyfe, I.M. (1998): A study of failure in small pressurized cylindrical shells containing a crack. NASA Report NASA/CR-1998-208454.

[118] Chen, C.-S., Wawrzynek, P.A. and Ingraffea, A.R. (1999): Crack growth simulation and residual strength prediction in airplane fuselages. NASA Report NASA/CR-1999-209115.

[119] Scheider, I., Schödel, M., Brocks, W. Schönfeld, W. (2006): Crack propagation analyses with CTOA and cohesive model: Comparison and experimental validation. Engng. Fracture Mech. 73, 252-263.

[120] Brocks, W. (2005): Cohesive strength and separation energy as characteristic parameters of fracture toughness and their relation to micromechanics. Struct. Integr. Durab. 1, 233-244.

[121] Windisch, M., Sun, D.-Z., Memhard, D. and Siegele, D. (2007): Defect tolerance assessment of ARIANE 5 structure on the basis of damage mechanics material modeling. Engng. Fracture Mech., This issue, xxx-xxx.

[122] Collins, R.A., Kimmins, S.T., Campassens, D. and Rodrigo, P. (2004): Advanced material and manufacturing techniques on future airbus aircraft, and the implications for fatigue and damage tolerance. Proc. 22th ICAF Symposium of the Int. Committee on Aeronautical Fatigue, Sheffield, U.K., 231-257.

[123] Schijve, J. (1995): Multiple-site damage in aircraft fuselage structures. Fatigue Fracture Engng. Mat. Struct. 18, 329-344.

[124] Liao, M., Shi, G. and Xiong, Y. (2001): Analytical methodology for predicting fatigue life distribution of fuselage splices. Int. J. Fatigue 23, S177-S185.

[125] Moussa, W.A. (1998): Risk-based reliability evaluation of multi-site damage in pipelines. Computers Ind. Engng. 35, 595-598.

[126] Pitt, S. and Jones, R. (2001): Compliance measurements for assessing structural integrity. Engng. Failure Analysis 8, 371-397.

[127] Harris, C.E., Newman, J.C., Jr., Piascik, R.S. and Starnes, J.H. (1998): Analytical methodology for predicting widespread fatigue damage onset in fuselage structures. J. Aircraft 35, 307-317.

[128] Swift, T. (1987): The effects of stress level, geometry and material on fatigue damage tolerance of pressurized fuselage structure. Proc. 14th ICAF Symposium of the Int. Committee on Aeronautical Fatigue, Ottawa, Canada, 1-77.

[129] Broek, D., Jeong, D.Y. and Thomson, D. (1994): Testing and analysis of flat and curved panels with multiple cracks. Proc. FAA/NASA Int. Symp. Advanced Structural Integrity Methods for Airframe Durability and Damage Tolerance, Hampton, VA, NASA Conf. Publ. 3274, 85-98.

[130] De Wit, R., Fields, R.J., Low, S.R., Harne, D.E. and Foecke, T. (1995): Fracture testing of large scale thin-sheet aluminium alloy. Nat. Inst. of Standards and Technology, Gaithersburg, MD, NISTIR Rep. 5661

[131] Nilsson, K.F. (1996): Elastic-plastic models for interaction between major crack and multiple small cracks. Proc. FAA/NASA Int. Symp. on Continued Airworthiness of Aircraft Structures, Atlanta. GA, 197-225.

[132] Smith, B.L., Saville, P.A., Mouak, A. and Myose, R.Y. (2000): Strength of 2024-T3 aluminium panels with multiple site damage. J. Aircraft 37, 325-331.

[133] De Wit, R., Fields, R.J., Mordfin, L., Low, S.R. and Harne, D. (1994): Fracture behavior of large-scale thin-sheet aluminium alloy. Proc. FAA/NASA Int. Symp. Advanced Structural Integrity Methods for Airframe Durability and Damage Tolerance, Hampton, VA, NASA Conf. Publ. 3274, 963-983.

[134] Koolloos, M.F.J., ten Hoeve, H.J., Grooteman, F.P. and de Koning, A.U. (2001): Analysis of residual strength of stiffened panels with multiple site damage. National Aerospace Laboratory NLR, The Netherlands, NLR Report NLR-TP-2001-342.

[135] Galatolo, R. and Nilsson, K.-F. (2001): An experimental and numerical analysis of residual strength of butt-joint panels with multiple site damage. Engng. Fracture Mech. 68, 1437-1461.

[136] Hsu, C.-L., Lo, J., Yu, J. Lee, X.-G. and Tan, P. (2003): Residual strength analysis using CTOA criteria for fuselage structures containing multiple site damage. Engng. Fracture Mech. 70, 525-545.

[137] Ciliato, G.D. and Carneiro, S.H.S. (2005): Analysis of the residual strength and link-up stress of aluminium plates with multi-site damage. 11th Int. Conf. Fracture, Milan.

[138] Ingraffea, A.R.: Predicting residual strength of as fuselage section with/without MSD and with/without corrosion. USAF Handbook for Damage Tolerant Design, Last update 2002, Problem No. FAC-2.

[139] Kim, J., Zhang, G. and Gao, X. (2007): Modeling of ductile fracture: Application of the mechanism-based concepts. Int. J. Solids Structures 44, 1844-1862.

[140] Congourdeau, F. and Journet, B. (2004): Damage tolerance of fuselage welded stiffened panels. Proc. 22th ICAF Symposium of the Int. Committee on Aeronautical Fatigue, Sheffield, U.K., 361-383.

[141] Farahmand, B. (2001): Fracture Mechanics of Metals, Composites, Welds, and Bolted Joints. Kluwer Academic Publ., Boston, Dordrecht, London, Chapter 6: Welded Joints and Applications, 274-303.

[142] Zhang, X., Irving, P., Edwards, L., Fitzpatrick, M., Sinclair, I. Lin, J. and Yapp, D. (2005): The influence of residual stress on design and damage tolerance of welded aircraft structures. Proc. 23rd ICAF Symposium of the Int. Committee on Aeronautical Fatigue, Hamburg, Germany, Vol. I, 1-265-281.

[143] Staron, P., Kocak, M., Williams, S. and Wescott, A. (2004): Residual stress in friction stir-welded Al sheets. Physica B 350, e491-e493.

[144] Ainsworth, R.A. (1986): The treatment of residual stresses in fracture assessments. Engng. Fracture Mech. 24, pp. 65-76.

[145] Dos Santos, J., Çam, G., Torster, F., Isfan, A., Riekehr, S., Ventzke, V., Koçak, M. (2000): Properties of power beam welded steels, Al- and Ti-alloys: Significance of strength mismatch. Welding in the World 44, 42-64.

[146] Çam, G., Koçak, M., Dos Santos, J. (1999): Developments in laser welding of metallic materials and characterization of the joints. Welding in the World 43, 13-25.

[147] Schwalbe, K.-H., Kim Y.-J., Hao, S., Cornec, A., Koçak, M. (1997): EFAM ETM-MM 96: The ETM Method for Assessing the Significance of Crack-Like Defects in Joints with Mechanical Heterogeneity (Strength Mismatch), GKSS Research Centre Geesthacht, GKSS Report 97/E/9.

[148] Seib, E. and Kocak, M. (2005): Fracture analysis of strength undermatched welds in thin-walled aluminium structures using the FITNET procedure. International Institute of Welding (IIW), IIW Doc. X-1577-2005.

[149] Nègre, P., Steglich, D. and Brocks, W. (2004): Crack extension in aluminium welds: a numerical approach using the Gurson-Tvergaard-Needleman model. Engng. Fracture Mech. 71, 2365-2383.

[150] Zerbst, U., Brocks, W., Heerens, J., Schödel, M., Scheider, I., Steglich, D., Seib, E., Cornec, A. and Schwalbe, K.-H. (2005): Failure assessment concepts fort thin-walled structures. Proc. 23rd ICAF Symposium of the Int. Committee on Aeronautical Fatigue, Hamburg, Germany, Vol. 1, 161-175.

[151] Higgins, A. (2000): Adhesive bonding of aircraft structures. Int. J. of Adhesion & Adhesives, 20, 367-376.

[152] Schijve, J. (1990): Crack stoppers and ARALL laminates. Eng. Fract. Mech., 37, 405-421.

[153] Schmidt, H.J. and Schmidt-Brandecker, B. (2003): Damage tolerance design and analysis of current future aircraft structure. Proc. AIAA/ICAS International Air and Space Symposium and Exposition: the next 100 years, Dayton, OH, AIAA 2003-2784.

[154] Rose, L. (1982): A cracked plate repaired by bonded reinforcements. Int. J. of Fracture, 18, 135-144.

[155] Baker, A. (1988): Crack patching: experimental studies, practical applications. In: Baker, A. and Jones, R. (eds.): Bonded Repair of Aircraft Structures, Martinus Nijhoff.

[156] Valoroso, N. and Champaney, L. (2006): A damage-mechanics-based approach for modeling decohesion in adhesively bonded assemblies. Engng. Fract. Mech. 73, 2774-2801.

[157] Carlberger, T. and Stigh, U. (2007): An explicit FE-model of impact fracture in an adhesive joint. Engng. Fract. Mech. 74, 2247-2262.

[158] Jensen, H.M. (2007): Interface fracture in adhesively bonded shell structures Engng. Fract. Mech. in press, doi:10.1016/j.engfracmech.2007.02.004.

[159] Heinimann, M.B., Bucci, R.J, Kulak, M. and Garrat, M. (2005): Improving the damage tolerance of aircraft structures through the use of selective reinforcement. Proc. 23rd ICAF Symposium of the Int. Committee on Aeronautical Fatigue, Hamburg, Germany, Vol. 1, 197-208.

[160] Zhang, X. and Li, Y. (2005): Damage tolerance and fail safety of welded aircraft wing panels. AIAA Journal 43, 1613- 1623.

[161] Colavita, M., Bowler, A., Zhang. X, and Irving, P.E. (2006): Adhesively bonded CFRP strap as fatigue crack growth retarders on AA2024-T3, SAMPE 2006, Long Beach.

[162] Zhang, X, Boscolo , M., Figueroa-Gordon, D., Allegri, G. and Irving, P. (2007): Fail Safe of Integral Aircraft Wing Structures Reinforced by Bonded Crack Retarders. Engng. Fracture Mech., This issue, xxx-xxx.

[163] Alderliesten, R. (2005): Fatigue Crack Propagation and Delamination Growth in Glare", Ph.D. Thesis TU Delft, Delft University Press.

[164] Boscolo, M., Allergi, G., Zhang, X. (2007): Design and Modeling of Selective Reinforcements for Integral Aircraft Structures. AIAA Paper 2007-2116, Proc. 48th AIAA/ASME/ASCE/AHS/ASC Structures, Structural Dynamics, and Materials Conference.

Symbols

a	crack length
a_o	initial crack depth before extension
a_{eff}	plastic zone corrected crack length (Eq. 4)
A_k, B_k	fit parameters Eq. (1)
B	specimen thickness (refers to t in components)
E	modulus of elasticity (Young's modulus)
E'	effective Young's modulus (= E for plane stress; = $E/(1-\nu^2)$ for plane strain)
$f(L_r)$	correction function for ligament yielding (SINTAP/FITNET)
f^*	damage variable (GTN damage model, Eq.12)
F	load (general term), also tensile force
F_j	validity criterion for K_{eff}-R curves according to GKSS and ESIS (Eq. 6)
F_Y	net section yield load (general term, also tensile yield force)
F_{YB}	yield load of base plate material (weldments)
F_{YM}	equivalent mismatch corrected yield load (strength mismatch joints)
F_{YW}	yield load of weld metal (weldments)
K	stress intensity factor (K factor)
K_I	mode I stress intensity factor
K_I^p	mode I stress intensity factor for primary loading
K_I^s	mode I stress intensity factor for secondary loading
K_p^s, ξ	auxiliary functions for the determination of V
K_{Ic}	plane strain fracture toughness (small scale yielding)
K_p	"ligament yielding corrected" K factor (Section 3.2, Fig. 21)
K_c	geometry dependent fracture toughness (Figure 1)
K_{eff}	plastic zone corrected K factor (Eq. 3)

K_R	crack resistance curve (R curve) curve based on K or K_{eff}
L_r	ligament yielding parameter (= $F/F_Y = \sigma_{ref}/\sigma_Y$)
L_r^{max}	plastic collapse limit L_r value
M	strength mismatch ratio (Eq. 22)
N	strain hardening exponent used in SINTAP/FITNET (Eq. 16)
q_1, q_2, q_3	fit parameters (GTN damage model; Eq. 12)
$R(\bar{\varepsilon})$	uniaxial true stress vs. plastic strain curve (GTN damage model; Eq. 12)
R,L	cylinder radius and the frame spacing of curves stiffened panels (Eq. 5)
$R_{p0.2}$	proof stress
R_m	uniaxial tensile strength
t	plate thickness
t_0	plate thickness referring to ASTM E399 plane strain conditions (Eq. 2)
T_0	maximum sustainable tensile stress (cohesive zone model)
V	correction factor for primary and secondary stresses interaction (Eq. 20)
W	specimen width
Y	geometry function of K factor solutions
β	bulging factor (Eq. 5)
δ_0	critical displacement (cohesive zone model)
δ	crack tip opening displacement (CTOD)
δ_5	CTOD definition according to Fig. (6); SINTAP/FITNET thin wall module
δ_e	elastic component of δ_5
Δa	stable crack extension
Δa_c	stable crack extension at instability
Δa_{max}	validity criterion for R curves (different approaches) Eqs. (6), (7) and (8)
φ	specimen orientation with respect to rolling direction (Fig. 22)

ψ	crack tip opening angle (CTOA)
Γ_0	separation energy (cohesive zone model)
λ	biaxial tension loading parameter (Fig. 23)
ν	Poisson's ratio
σ	stress
σ_{kk}	hydrostatic (mean) stress
σ_{eq}	equivalent stress
σ_{ref}	net section reference stress
σ_Y	yield strength (general term)
σ_{YB}	yield strength of the base plate material (weldments)
σ_{YW}	yield strength of the weld metal (weldments)

Abbreviations

ASTM	American Society for Testing and Material
BS 7910	failure assessment standard (British Standard)
C(W)	crack line wedge loaded specimen
C(T)	compact tension specimen
CDF	crack driving force
CFK	carbon fibre reinforced plastic
CTOA	crack tip opening angle
CTOD	crack tip opening displacement
ESIS	European Structural Integrity Society
DE(T)	double edge tension specimen
FITNET	Fitness for Service Network (European)
FML	fiber metal laminate

GKSS	GKSS Research Centre
GTN	Gurson-Tvergaard-Needleman model
ISO	International Standards organisation
M(T)	middle cracked tension specimen
MSD	multi site damage
R6	R6 procedure (British Energy Nucleation Ltd.)
R curve	crack resistance curve
SINTAP	Structural Integrity Assessment Procedure (European)
2D	two dimensional
3D	three dimensional